NASA TECHNICAL MEMORANDUM

NASA TM X-68096

NASA TM X-68096

OPTIMIZATION OF ELECTROSTATIC DUAL-GRID BEAM-DEFLECTION SYSTEM

by W. R. Hudson, W. C. Lathem,
J. L. Power, and B. A. Banks
Lewis Research Center
Cleveland, Ohio

June, 1972

This information is being published in preliminary form in order to expedite its early release.

OPTIMIZATION OF ELECTROSTATIC DUAL-GRID BEAM-DEFLECTION SYSTEM

by W. R. Hudson, W. C. Lathem, J. L. Power, and B. A. Banks

Lewis Research Center

E-7012

SUMMARY

Tests were performed to minimize accelerator grid erosion of a 5-cm diameter Kaufman ion thruster due to direct beam impingement. Several different screen hole diameters, pillow-shape-square screen holes, and dished screen grids were tried. The optimization was accomplished by copper plating the accelerator grid before testing each grid configuration on a thruster for a 2-hour run. The thruster beam sputtered copper and molybdenum from the accelerator grid where the beam impinged. The observed erosion patterns and measured accelerator currents were used to determine how to modify the accelerator system. The lowest erosion was obtained for a 50-percent open area pillow-shape-square-aperture screen grid, dished 0.043 centimeter convex toward the accelerator grid, which was positioned with the center of the screen grid 0.084 centimeter from the accelerator grid. During this investigation the accelerator current was reduced from 120 to 55 microamperes and was also more uniformly distributed over the area of the accelerator grid.

INTRODUCTION

In the 1970's, increasing use of orbiting spacecraft for Earth resources studies, meteorology, and communications is planned (ref. 1). Many of these satellites will have stringent, long duration station-keeping and attitude control requirements. As satellite lifetime increases, the propellant requirements make the relatively higher

specific impulse ion thruster a highly competitive alternative to cold gas and chemical type thrusters. An analysis of a 7-year north-south station-keeping mission by Free (ref. 2) has indicated the superiority of the ion thruster.

The Lewis Research Center has worked for several years on a 5-cm Kaufman thruster with the durability (lifetime) and specific impulse to meet these general requirements. The Lewis 5-cm thruster program has been described in references 3 and 4. Hughes Research Laboratories was awarded Contract NAS3-15483 to design and build a structurally integrated mercury bombardment ion thruster (ref. 5).

Recent development of ion thrusters with beam deflection capability enhances their utility, because both station-keeping and attitude control functions can be performed. Hughes Research Laboratories personnel have investigated several beam deflection systems under Contract NAS3-14058. The results are described in references 6 and 7. The deflection system that was chosen as the primary method is the electrostatic dual grid system. The electrostatic dual grid system can deflect the beam about two orthogonal axes by electrostatic biasing of the grid elements. An early version of the electrostatic dual grid system has been run for 1000 hours on a 5-cm diameter Kaufman thruster, reference 8. Figure 1 is a photograph of the electrostatic dual grid system.

It became apparent during the 1000-hour run that erosion of the accelerator grid by direct impingment of the beam was a major problem. Direct impingement is a problem for the electrostatic dual grid system because of the relatively large thickness of the accelerator grid (table I) and the limited number of apertures. For the double flat grids, dished grids, and translating screen grid acceleration systems, erosion by direct impingement is insignificant.

This paper describes a series of experimental changes designed to reduce the accelerator grid erosion due to direct ion impingement of the beam. Screen grid geometry and position with respect to the accelerator grid were varied to minimize accelerator current at a constant

25 mA beam current. Several different screen hole diameters, pillow-shape-square hole screen holes, and dished screen grids were investigated. The accelerator grid was the same for all tests.

To reduce the time required for the erosion measurements needed to evaluate each configuration, the accelerator grid was copper plated. The grid was then mounted on a 5-cm prototype engine and typically run for a 2-hour period. The copper plating was very quickly sputtered off the grid where direct ion impingement occurred. Following the 2-hour runs, the accelerator grid was photographed and studied under a microscope. The level of accelerator current and the observed erosion patterns were used to decide what changes to make in the accelerator system.

APPARATUS AND PROCEDURES

The beam deflection system (fig. 1) was mounted on a 5-cm Kaufman ion thruster (fig. 2) for the erosion studies. The thruster has been described in detail in references 3 and 4. Enclosed hollow cathodes were used for both the main cathode and the neutralizer. The neutralizer was positioned 4.0 cm downstream, 4.0 cm from the edge of the active area of the grid and pointed at an angle of 10^{o} radially inward with respect to the axis of the thruster. The electrostatic deflection accelerator grid (fig. 1) is made up of molybdenum strips 0.254 cm wide and 0.013 cm thick. The resulting apertures were 0.343 cm square. Accelerator grid open area was 53 percent. Each of the four different screen grids tested contained a square array of holes on a 0.445 cm center-to-center spacing. Screen grids having circular holes of 0.392 cm, 0.318 cm, and 0.294 cm in diameter were tested. The fourth screen grid had pillow-shape-square screen holes (fig. 3). Reference 9 describes the development of the pillow-shape-square screen grid apertures. The screen holes are contoured so that a square

beamlet is produced. Table I is a summary of test configurations. The symbols used to designate the dimensions of the screen and accelerator grids are indicated. Each screen grid was carefully alined with respect to the accelerator apertures before each test.

The experiments were performed in a 4.5 m long by 1.5 m diameter vacuum facility (ref. 10). A vertical insulator (50 percent Al_2O_2, 50 percent SiO_2) covered metal target was placed midway to divide the facility. The insulating material decreased the total amount of back-sputtered metal arriving at the thruster.

Most of the experimental runs were for a period of 2 hours. Before the main discharge was ignited and the high voltage supplies turned on, the main cathode and the neutralizer were both run for a period of at least 2 hours. Figure 4 shows how the thruster parameters varied during a typical run. During the warmup period, the mercury flow rates to both the cathodes were measured at intervals of 10 minutes. The main discharge was not turned on until the mercury flow rates were constant at the desired values for 30 minutes. The mercury was supplied to the vaporizers from 0.5 mm diameter capillary burettes. Mercury flow rates could then be determined precisely from the change in height of the mercury column with time. Iron-constantan thermocouples were used to monitor the temperatures of the main cathode vaporizer and the neutralizer vaporizer.

After the 30-minute stable flow period, the discharge was ignited and the high voltage supplies were turned on (V_I = 1200 volts and V_A = -1200 volts unless otherwise specified). The thruster was operated at discharge-chamber propellant utilization efficiencies between 61 and 74 percent. The beam current and utilization efficiencies were not corrected for double ionization. The discharge losses were typically above 800 eV/ion. The beam current was held at 25 mA. The main cathode was operated with the keeper supply turned off.

After each run, the grid was removed from the thruster for examination. The areas where copper and molybdenum were sputtered off the

accelerator grid were documented and photomicrographs of particular areas were taken. The level of accelerator current and the erosion pattern were used to decide what changes to make in the accelerator system.

Copper Plating Procedure

The detailed procedure by which the accelerator grid system, made of high purity, arc-cast molybdenum, was electroplated with copper prior to thruster testing is given in Appendix B. The procedure by which the copper was stripped from the grid system in preparation for replating is also given in Appendix B. The thickness of the copper plating for the erosion tests was estimated to be 0.5 to 1.0×10^{-4} cm, or roughly 0.4 - 0.8 percent of the accelerator strip thickness. The electroplated copper displayed a uniform, smooth, bright copper appearance, was of uniform thickness on all surfaces and edges of the accelerator grid strips, and was very adherent and resistant to removal by scratching or abrasion.

Hydroforming of Dished Grids

A sketch of the hydroforming apparatus is shown in figure 5. Reference 11 gives a complete description of the hydroforming techniques. The circumference of the grid is clamped rigidly with an acetate sheet between the grid and the hydraulic fluid inlet. A hydraulic jack is used to pressurize the fluid and hydroform the grid. The resulting grid was approximately spherical in shape over the 5 cm diameter. A dial indicator was used to measure the amount of dishing. The grid used in this experiment was dished to a height h of 4.3×10^{-2} cm (fig. 5).

RESULTS AND DISCUSSION

Six different screen grid-accelerator grid configurations were tested. The first three tests were on screen grids with circular holes. The last three runs used a screen grid with pillow-shape-square holes (ref. 9). In the fifth and sixth runs, the pillow-shape-square hole screen grid was dished. Table I contains a summary of the test configurations, accelerator current and discharge losses. The tests are described below in chronological order.

The first screen grid tested had 0.392 cm diameter circular holes and 61 percent open area. The screen grid was 0.127 cm from the upstream side of the accelerator grid. The average propellant utilization was 64 percent and the discharge losses averaged out at 416 eV/ion. The accelerator current held constant at 100 μA over the 2-hour run. Examination of the grid after the run revealed that several accelerator apertures in the center of the grid were suffering direct impingement. Figure 6 is a photograph of a typical example of direct impingement. The dark parabolically shaped region in the center of the tab on the accelerator strip is the region where direct impingement has sputtered the copper off the tab. The lighter regions are still copper plated. In some cases of heavy erosion, in which the copper plate was completely eroded through, the underlying molybdenum was sputtered onto the copper plating on the sides of the accelerator aperture where no impingement occurred. In particular runs, some apertures showed erosion on two, three, and four sides.

Next, the 50 percent open area pillow-shape-square aperture screen grid was tested. It was 0.140 cm from the accelerator grid. The propellant utilization was 66 percent and the discharge losses were 836 eV/ion. The pillow-shape-square screen grid operated with an accelerator current of 85 μA, an improvement of 15 percent. The direct impingement still occurred in the center apertures of the accelerator grid, but was spread out over more apertures.

Because reducing the open area of the screen grid resulted in lower accelerator current, the next test was made with a screen grid having a 40 percent open area and 0.318 cm diameter circular holes. The distance between the screen and accelerator grid was 0.122 cm. Discharge loss of 834 eV/ion and a propellant utilization of 63 percent were obtained. The accelerator current decreased from 120 μA at the start of the run to 100 μA at the end of the run. The average measured accelerator current was 106 μA. The beam again sputtered copper off the center apertures of the accelerator grid.

In the next test a screen grid with 35 percent open area and 0.295 cm diameter holes was employed. The grid spacing was kept at 0.122 cm. The thruster performance was adversely affected by the lower open area. The propellant utilization was 62 percent and the discharge losses were averaged 915 eV/ion for the 2-hour run. The accelerator current started out at 170 μA, went as low as 120 μA, and averaged out at 138 μA. The direct impingement was concentrated very heavily in the center apertures of the accelerator grid.

These tests showed that decreasing the screen open area did not significantly reduce accelerator impingement current. In an attempt to improve on the results achieved in the second test by dishing the 50 percent open area, a pillow-shape-square aperture screen grid was dished. It was hoped that dishing the grid convex toward the accelerator grid would redistribute the beam current more uniformly over the grid and also improve the focusing in the center of the grid where most of the direct impingement had occurred. The 50 percent open area pillow-shape-square aperture screen grid was hydroformed so that the center of the grid was permanently displaced 0.043 cm. The distance between the accelerator grid and the center of the screen was 0.097 cm. This screen configuration was a definite improvement. The thruster operated at a propellant utilization 64 percent and discharge losses 718 eV/ion. The accelerator current averaged out at 90 μA and the direct impingement was moved from the center of the accelerator grid toward the edges. The

impingement was particularly heavy on one accelerator strip so it was manually repositioned and the test was repeated after a one-half hour warmup period. The thruster was run for 2 hours at an average propellant utilization of 70 percent and with discharge losses of 937 eV/ion. The accelerator current was in the 70 to 75 μA range and the impingement was on the outer apertures of the accelerator grid. This screen grid was also run with the dish concave toward the accelerator grid. The resulting accelerator current was 215 μA.

Because it was thought that dishing the screen grid improved the focusing in the center apertures of the accelerator grid by moving the center of the screen grid closer to the accelerator grid, in the next test the whole screen grid was moved 0.012 cm closer to the accelerator grid. This change was achieved by shimming the screen grid 0.012 cm away from the pole piece. The center of the screen grid was then 0.084 cm from the accelerator grid and the edge of the screen was 0.127 cm from the accelerator grid. With the usual net accelerating voltage V_I at +1200 and the usual accelerator voltage V_A at -1200 volts, the accelerator current was 80 μA. During the last hour of this run, the net accelerating voltage was raised to +1600 volts and the accelerator voltage set at -800 volts. These values were chosen to minimize the accelerator current. The thruster was run at a propellant utilization efficiency of 74 percent and discharge losses of 1102 eV/ion. The accelerator current was as low as 55 microamperes and averaged 65 μA.

The final run was a repeat of the previous run. In this run, the final optimization of the grid system was performed. The thruster was run at the highest possible propellant utilization, and the optimization of V_I and V_A was repeated, V_I equal to +1600 V and V_A equal to -800 V was again obtained. The neutralizer flow was minimized, and the neutralizer coupling voltage was minimized (to a value of 10 volts) by increasing the neutralizer keeper current from 0.5 A to 0.6 A. The thruster was run for 2 hours, but unlike the previous runs, the operating

conditions were varied during the first hour. During the last hour of the run, the thruster ran steadily at 73 percent utilization and with discharge losses of 1445 eV/ion. The accelerator current was at 55 μA during this hour. This value is 0.22 percent of the 25 mA beam current. Most of the erosion damage occurred at or near the outer aperture of the accelerator grid, and a considerable amount of the damage probably occurred during the first hour of the run when the accelerator current was as high as 130 μA. Comparison between the original grid (test 1) and the final configuration shows a 45 percent reduction in accelerator impingement current. The final configuration had the additional beneficial result of spreading the direct impingement over a larger area of the grid.

CONCLUSION

Tests employing several different screen grids and different spacings between screen and accelerator grids were performed to minimize the erosion of the accelerator grid by direct impingement of the beam. The lowest erosion was obtained with a 50 percent open area pillow-shape-square aperture screen grid, dished 0.043 cm convex toward the accelerator grid. The center of the screen was 0.084 cm from the accelerator grid. The 55 μA of direct impingement was spread over a large area of the grid. This value is 0.22 percent of the 25 mA beam current. The accelerator current of the original configuration was 100 μA and the direct impingement was concentrated in the center apertures of the accelerator grid. A 45 percent reduction in accelerator current was achieved and the remaining ion impingement spread over a large area of the grid. The optimization in these tests was greatly speeded by the technique of copper plating the accelerator grid prior to testing. The copper plating was sputtered off the regions of the accelerator grid where direct impingement occurred. The pattern, distribution, and

intensity of the erosion were used to decide what modifications to make in the accelerator system.

Lewis Research Center,
National Aeronautics and Space Administration,
Cleveland, Ohio, June 1, 1972.

APPENDIX A

SYMBOLS

h	height of dish
J_A	acceleration current
J_B	beam current
J_{CH}	cathode tip heater current
J_{CK}	cathode keeper current
J_{CV}	cathode vaporizer current
J_I	discharge current
J_{NH}	neutralizer tip heater current
J_{NK}	neutralizer keeper current
J_{NV}	neutralizer vaporizer current
$\dot{m}_c$	propellant flow rate (equivalent mA)
V_A	accelerator voltage
V_{CH}	cathode tip heater voltage
V_{CK}	cathode keeper voltage
V_{CV}	cathode vaporizer voltage
V_G	coupling voltage
V_I	net accelerating voltage
V_{NH}	neutralizer tip heater voltage
V_{NK}	neutralizer keeper voltage
V_{NV}	neutralizer vaporizer voltage
T_{CV}	cathode vaporizer temperature
T_{NV}	neutralizer vaporizer temperature
ΔV_I	discharge voltage
η_u	propellant utilization

Notation for screen and accelerator apertures are defined in table I.

APPENDIX B

COPPER ELECTROPLATING AND STRIPPING PROCEDURES

Cleaning Prior to Electroplating

All operations were performed on the demounted accelerator assembly, consisting of the anode pole piece, the screen grid, the accelerator grid strip system, and the accelerator grid mounting insulators. This assembly was rinsed thoroughly in CH_3CCl_3 (NA-500), then ultrasonically cleaned in high purity CF_3CCl_3 at least twice for periods of 15 minutes or longer, and finally rinsed thoroughly in C. P. acetone.

Electroplating Procedure

The plating solution was prepared by dissolving 83.5 g concentrated H_2SO_4 and 67 g $CuSO_4 \cdot 5H_2O$ (technical grade) per liter of solution, made up with distilled water. Plating was done in a crystallizing dish 15 cm in diameter by 7.5 cm high. A square copper sheet approximately 10 cm on each side was used as the anode. This sheet had holes in it to facilitate solution circulation. The total (immersed) anode area was ~190 cm^2. The anode was cleaned before use by washing it with a detergent and water, rinsing it with acetone, stripping it to a bright appearance by brief immersion in fairly concentrated HNO_3, and finally rinsing it in water. The anode was mounted horizontally at about midheight in the plating bath (via tabs supporting it from the dish rim). The demounted accelerator assembly, after cleaning, was supported horizontally in the plating bath with the grids facing down. The assembly was centered above the anode and parallel to it at a closest distance of about 0.65 cm. (The anode to grid distance was found not to be critical.) The four tabs for the electrical leads to the four sets of accelerator grid slats were electrically connected together to form a common cathode lead. This

lead was connected to the cathode lead from a current-voltage controlled direct current power supply. The anode lead from the supply was connected to the copper anode. The accelerator grid system was maintained electrically isolated from the rest of the accelerator assembly.

The plating bath was partially filled with the plating solution and the bath carefully leveled so that the accelerator grid was horizontal and parallel to the solution surface. More plating solution was added until the accelerator grid slats were just totally immersed in the solution. Throughout the plating procedure the plating solution was maintained at room temperature and stirred (magnetically) at a moderate rate. The immersed grid system was allowed to soak for about 5 minutes without applied voltage, then up to a maximum of 0.6 V plating potential was applied. The electroplating was conducted at cathode current densities of 22 - 25 mA cm^{-2} (3.5 - 4.0 A total current over a plating area of $\sim$160 cm^2). Plating was typically continued for 60 - 70 seconds, during which time the plating voltage decreased somewhat as the plating current was held constant. The plating thickness could be estimated from the cathode current density and the plating time, assuming near unity current efficiency. The plate thickness calculated under the above conditions was $\sim 5 \times 10^{-5}$ cm. At the conclusion of the electroplating, the accelerator system was rinsed copiously with water and then with chemically pure acetone. The plating solution, which is not depleted or contaminated during the plating process, could be repeatedly reused.

During the plating procedure, precautions were taken (not always successfully) to keep the plating solution from contacting the iron anode pole piece of the accelerator assembly. Any such contact caused rapid attack on the iron and spontaneous copper plating on all the metal parts electrically connected to the pole piece and contacted by the solution.

Stripping Procedure

Following testing, the demounted accelerator assembly was thoroughly washed in CH_3CCl_3(NA-500) and chemically pure acetone. The stripping solution used was 5.2 M (0.33 concentrated) HNO_3, contained in a shallow culture dish. The accelerator system, held horizontally, was lowered so just the accelerator grid slats were immersed in the stripping solution. The stripping, done at room temperature with slight agitation, was continued until the copper plate was visibly removed and a brown coloration was seen in the solution, indicating significant attack on the molybdenum of the slats. The accelerator system was then immediately removed and rinsed copiously with water. For an $\sim 5 \pm 10^{-5}$ cm thick copper plate ~20 seconds stripping time was required. (The same thickness plate required ~3 - 5 seconds stripping time in 6.3 M HNO_3 or ~8 minutes in 3.9 M HNO_3.) For thicker copper plates, two or more fresh batches of the stripping solution were used during the stripping.

The brown-black molybdenum oxide coating produced on the molybdenum grid assembly components by the above operation was removed by a second stripping step, conducted in the same manner, using concentrated HCl containing ~0.5 M HNO_3. About one minute or less of stripping was required in this step, following which the accelerator assembly was thoroughly rinsed with water.

The molybdenum accelerator system components, after the above two-step stripping, had regained their original dull, light gray appearance, though their surfaces appeared somewhat etched. The amount of molybdenum removed from them during the stripping operations was sufficiently small, however, that the 0.013 cm thick accelerator grid slats were not observed to be noticeably thinner at the conclusion of the reported series of tests, despite numerous electroplatings and strippings by the above procedures.

REFERENCES

1. Anon.: A Survey of Space Applications. NASA SP-142, 1967.

2. Free, B. A.: Economic Tradeoff Studies for Electric Propulsion Missions on Communications Satellites. Paper 71-683, AIAA, June 1971.

3. Reader, Paul D.; Nakanishi, Shigeo; Lathem, Walter C.; and Banks, Bruce A.: A Submillipound Mercury Electron Bombardment Thruster. J. Spacecraft Rockets, vol. 7, no. 11, Nov. 1970, pp. 1287-1292.

4. Nakanishi, S.; Lathem, W. C.; Banks, B. A.; and Weigand, A. J.: Status of a Five-Centimeter-Diameter Ion Thruster Technology Program. Paper 71-690, AIAA, June 1971.

5. Hyman, Julius, Jr.: Design and Development of a Small Structurally Integrated Ion Thruster System. Hughes Research Labs. (NASA CR-120821), Oct. 1971.

6. Collett, C. R.; King, H. J.; and Schnelker, D. E.: Vectoring of the Beam from Ion Bombardment Thrusters. Paper 71-691, AIAA, June 1971.

7. King, H. J.; Collett, C. R.; and Schnelker, D. E.: Thrust Vectoring Systems. Part I: 5 cm Systems. Hughes Research Labs. (NASA CR-72877), 1970.

8. Lathem, Walter C.: A 1000-Hour Test of a Dual Grid, Electrostatic Beam Deflection Accelerator System on a 5-Centimeter-Diameter Kaufman Thruster. NASA TM X-67908, 1971.

9. Byers, David C.; and Banks, Bruce A.: Beam Focusing Characteristics of Variously Shaped Grid Holes. NASA TM X-67922, 1971.

10. Keller, Thomas A.: NASA Electric Rocket Test Facilities. Seventh National Symposium on Vacuum Technology Transactions. C. Robert Meissner, ed., Pergamon Press, 1961, pp. 161-167.

11. Rawlin, V. K.; Banks, B. A.; and Byers, D. C.: Design, Fabrication, and Operation of Dished Accelerator Grids on a 30-cm Ion Thruster. Paper 72-486, AIAA, Apr. 1972.

TABLE I. - TABULAR SUMMARY OF THE TEST CONFIGURATIONS AND RESULTS

	Grid configurations					
	Flat, circular aperture screen grid	Flat, pillow-shape-square screen grid	Flat, circular aperture screen grid		0.043 cm dished, pillow-shape square screen grid	
Percent open area	61	50	40	35	50	50
d_a, cm	0.343	0.343	0.343	0.343	0.343	0.343
d_s, cm	0.393	0.318	0.318	0.294	0.318	0.318
t_a, cm	0.254	0.254	0.254	0.254	0.254	0.254
t_s, cm	0.051	0.038	0.059	0.059	0.038	0.038
Y grid edge	0.127	0.140	0.122	0.122	0.140	0.127
Y grid center	0.127	0.140	0.122	0.122	0.097	0.084
ΔV_I, V	46	44	35	34	48	55
η_u, percent	64	66	63	62	70	74
eV/ion	416	836	834	915	937	1,102
Minimum J_A, μA	100	85	100	120	70	55
$\dot{m}_c$	39.3	37.9	39.6	40.7	35.5	32.8

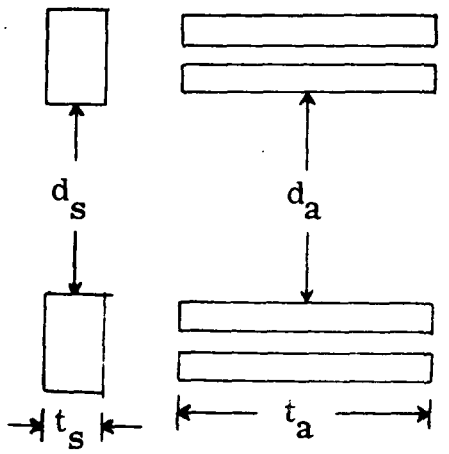

Dimensional notation for single screen and accelerator aperture

d_a - major accelerator grid dimension

d_s - major screen grid diameter

t_a - thickness accelerator grid

t_s - thickness screen grid

y - spacing between accelerator grid and screen grid

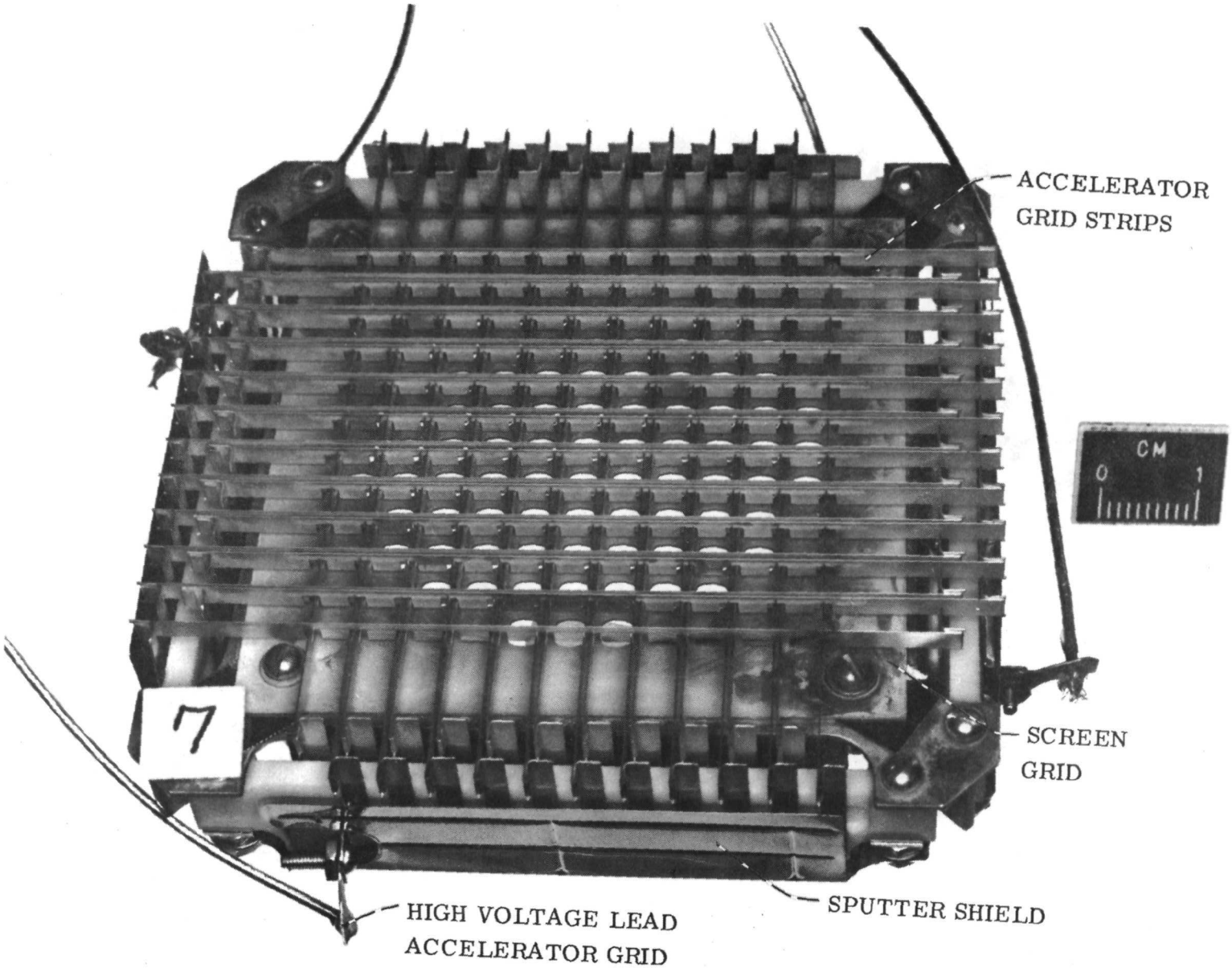

Figure 1. - The electrostatic dual grid beam deflection system.

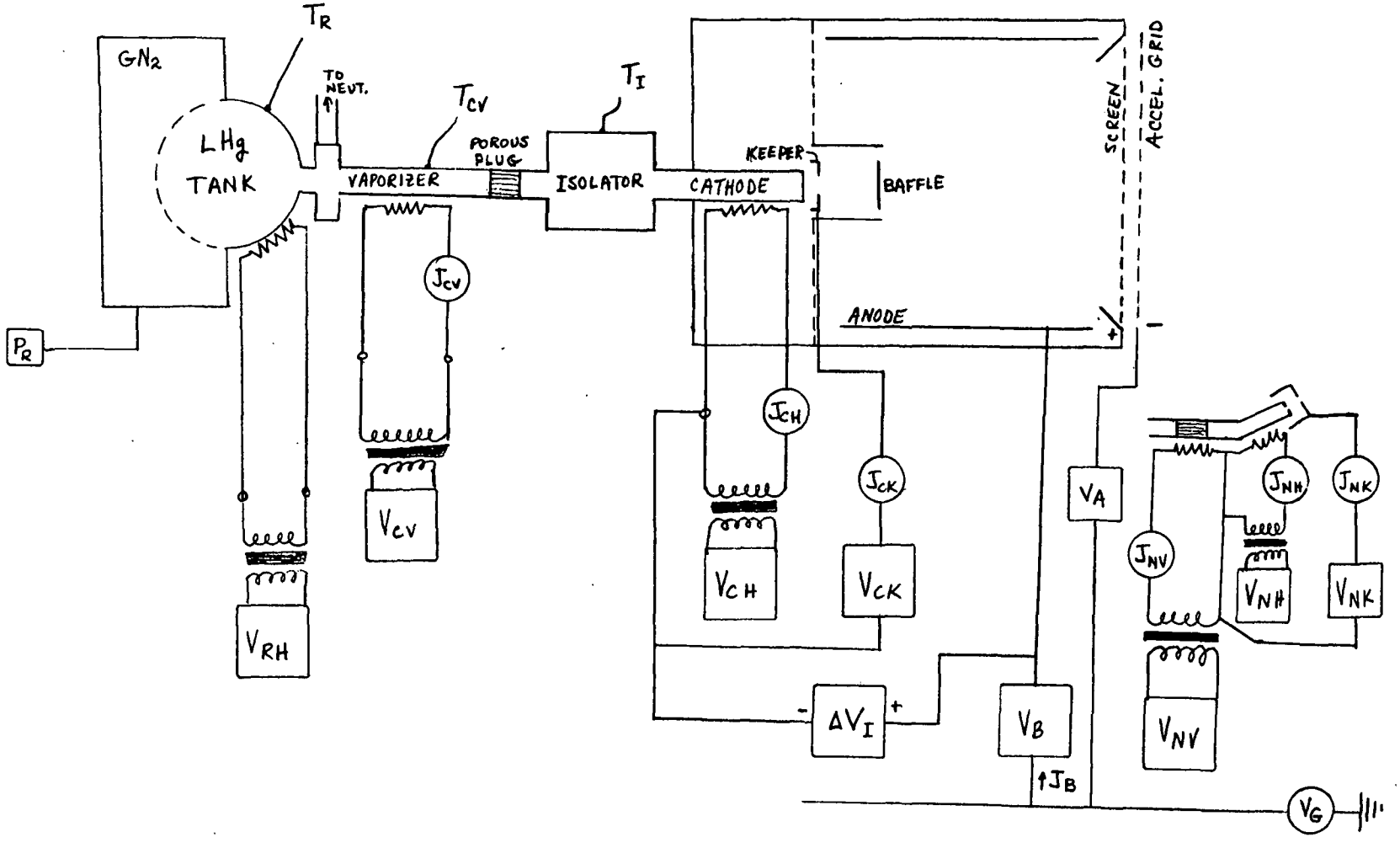

Figure 2. - Ion thruster engine parameters.

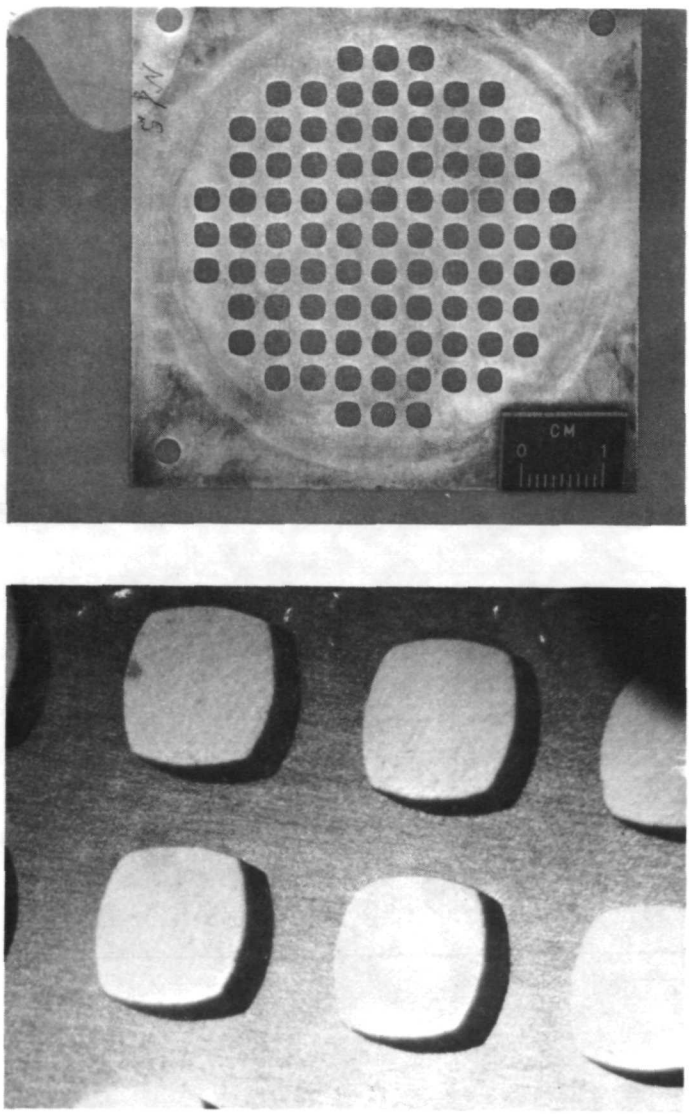

Figure 3. - Photograph of pillow-shape-square screen grid and a 7.5 power microscope picture, individual apertures.

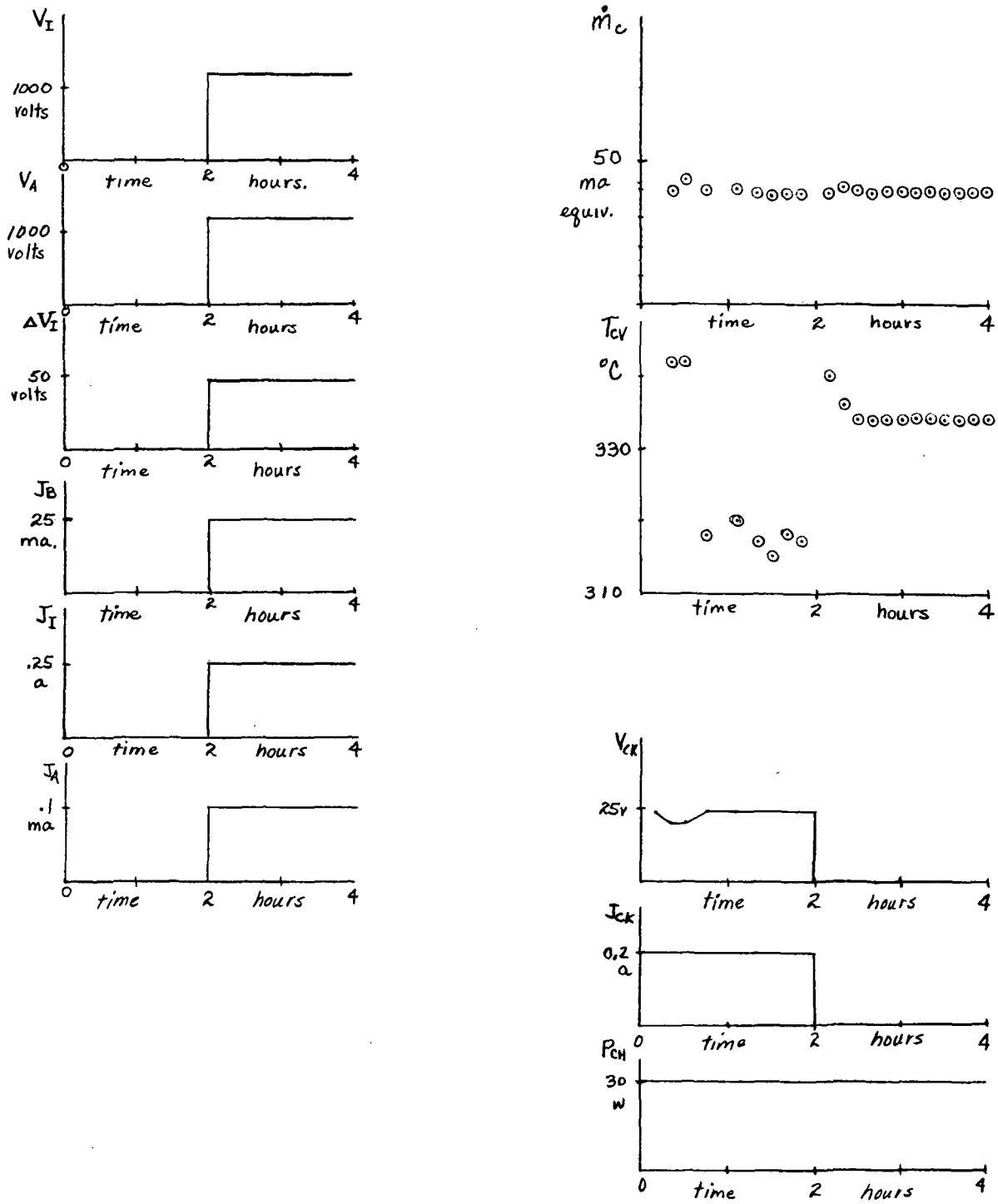

Figure 4. - Variation of thruster parameters during experimental run and warmup period.

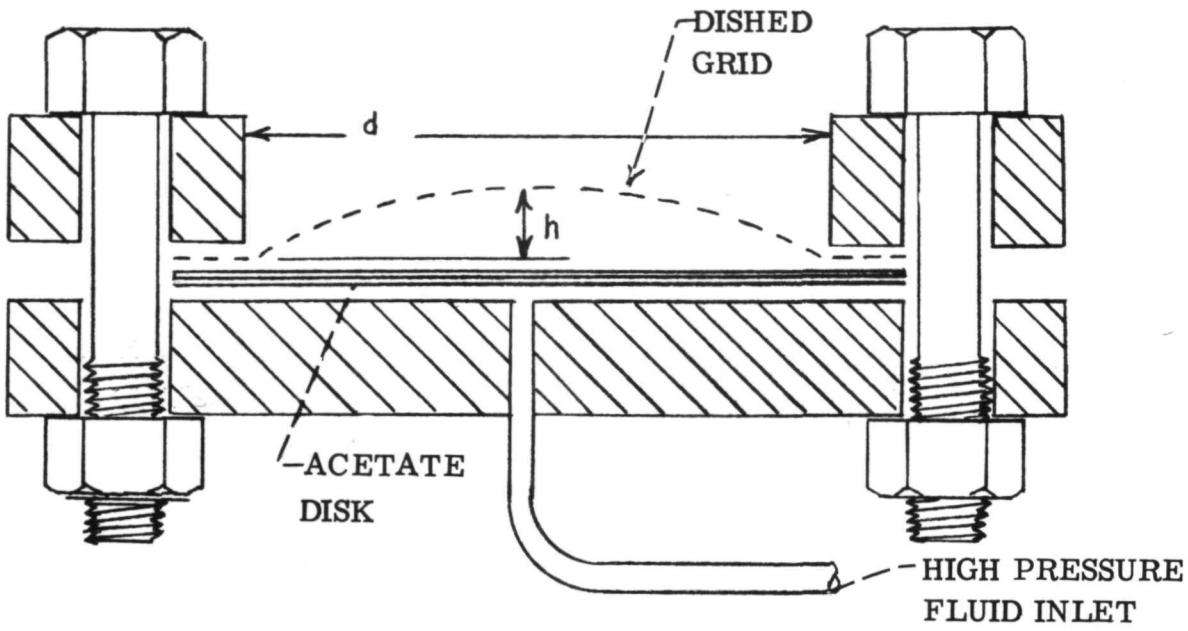

Figure 5. - Hydroforming apparatus used for fabrication of dished grids.

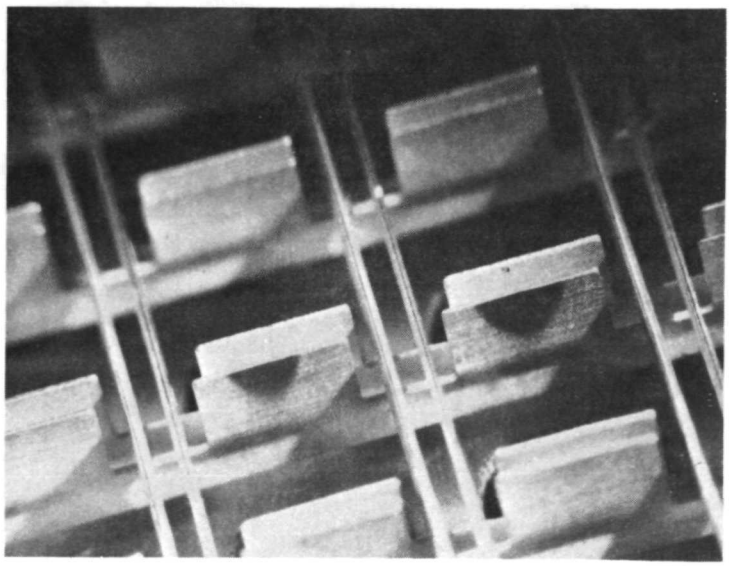

Figure 6. - Photograph showing region where direct impingement has sputtered the copper off the accelerator strips.

Anisotropies in the Interplanetary Intensity of Solar Protons $E_p > 0.3$ MeV*

by

WILLIAM G. INNANEN**
and
JAMES A. VAN ALLEN

Research was sponsored in part by the Office of Naval Research under contract N00014-68-A-0196-0003.

Department of Physics and Astronomy
THE UNIVERSITY OF IOWA
Iowa City, Iowa

Anisotropies in the Interplanetary Intensity of Solar Protons $E_p > 0.3$ MeV*

by

WILLIAM G. INNANEN**
and
JAMES A. VAN ALLEN

Department of Physics and Astronomy
The University of Iowa
Iowa City, Iowa 52240

June 1972

* Research supported in part by the National Aeronautics and Space Administration under contract NAS5-9076 with Goddard Space Flight Center and by U. S. Office of Naval Research contract N00014-68-A-0196-0003.

** NASA Pre-Doctoral Trainee 1965-1968.

ABSTRACT

From a much larger body of data on solar protons $E_p > 0.3$ MeV obtained by Explorer 35 since July 1967, the following ten events were selected for the detailed study of intensity vs time and of angular distributions of intensity in interplanetary space near the earth: November 18, 1968; August 9, 1967; May 13, 1969; January 24, 1969; March 21, 1969; June 25, 1970; January 31, 1970; July 1, 1970; November 27, 1967; and July 6, 1970. The bases of selection were that the events be of adequate intensity for statistically satisfactory study and that they be "simple"--that is, reasonably attributable to a single solar flare so that their time histories were not complicated by overlapping emissions of particles. The principal findings for these events are as follows:

(a) The time-integrated value of the net anti-solar flux of protons $E_p > 0.3$ MeV over these several events ranged from 10^{33} to 10^{35} protons per steradian, the result being expressed as the number of particles per unit solid angle at 1 AU referenced to the sun as the apex of the infinitesimal solid angle. The events caused by flares near the central meridian of the sun

usually produced the greatest values of time-integrated outward flux. though the general significance of this result is limited since the ten selected events may not constitute a representative sample of solar events.

(b) An anisotropy vector (C, δ) in the ecliptic plane has been calculated as a function of time from the detailed angular distribution data. Following earlier work on much more energetic solar protons $7.5 < E_p < 45$ MeV by McCracken et al. [1968, 1971] and theoretical guidance by Forman [1970a, 1970b] the observed anisotropy vector was resolved into two components: one radial from the sun, C_R, and one along the local magnetic field line, C_M. These components are given as a function of time.

(c) During the early phases of the events, C_M is the dominant component of the anisotropy. Later, during the decay phases, the anisotropy vector is only weakly correlated with the magnetic field direction.

(d) Throughout most of the events (one significant exception), the radial component of the anisotropy is uniformly positive (outward from the sun) and of magnitude in good agreement with theoretical values of the convective anisotropy calculated from observed values of solar wind velocity and spectral indices.

(e) The decay phase value of the field aligned component of the anisotropy vector, assumed to be diffusive in nature, is negative in many cases, and yields a value of $K \cdot \nabla U / U$ as great

as 7×10^{20} cm^2/sec - AU, where K is the diffusion tensor and U is the particle density. In other cases the anisotropy during this period is slightly positive or indistinguishable from zero.

(f) The field aligned component of the anisotropy in the rising phase of some events diminishes over a period of a day or two down to the decay phase values. A typical peak magnitude of this component, if interpreted as being caused by diffusive transport of protons, yields a value of $K \cdot \nabla U/U$ of -3×10^{21} cm^2/sec - AU.

(g) The fact that strong field aligned proton anisotropies are observed for events produced by eastern flares indicates that interior to the earth's orbit the particle distribution has been spread over a broad range of solar longitude.

INTRODUCTION

The frequent solar emission of protons in the energy range down to and below 1 MeV was first established in 1961 by measurements on Injun 1 [Pieper et al., 1962] and in 1962 by measurements on Mariner 2 [Van Allen and Frank, 1962] [Van Allen et al., 1964]. Such events have now been monitored on a nearly continuous basis over a full solar activity cycle of 11 years by University of Iowa equipment on a series of earth satellites and space probes. The most comprehensive measurements in the sub-MeV energy range over an extended period of time have been conducted by Explorer 33 from July 1, 1966 to November 1, 1971 and by Explorer 35 beginning on July 19, 1967 and continuing at the present date. A technique for measuring the angular distribution of the intensity of protons $E_p > 0.3$ MeV in interplanetary space was first introduced on Explorer 33, whose spin axis was approximately in the ecliptic plane. The same technique was applied to Explorer 35, with more valuable results because of the more favorable orientation of the spin axis.

The present paper gives the first detailed studies of the angular distributions of solar proton intensities in interplanetary space in the low energy range $E_p \geq 0.3$ MeV. Solar proton intensity

data from two channels of the University of Iowa solid state detector on Explorer 35 [Van Allen and Ness, 1969] are used for this purpose. Explorer 35 has been in lunar orbit since July 22, 1967. The spacecraft has an eccentric orbit with a period of approximately 11.5 hours and spins about an axis which is oriented to within 7° of the perpendicular to the ecliptic plane. The solid state detector has its axis perpendicular to the spin axis so that it sweeps around the ecliptic plane with the spin period of about 2.5 seconds. The single element detector has four channels: P1, which is sensitive primarily to protons with energies 0.322 to 6.3 MeV; P2, sensitive to protons with energies 0.478 to 3.0 MeV; P3, which is sensitive only to particles of $Z \geq 3$; and P4, which is sensitive primarily to alpha particles in the energy range 2.0 to 10.2 MeV.

Counts from the channels of interest here, P1 and P2, are accumulated in a spin averaged mode. In addition, counts from the P1 channel are divided into four equal sectors in the ecliptic plane. The longitude ranges of the detector's axis in spacecraft centered solar ecliptic coordinates during accumulation of counts in the respective sectors are as follows: Sector I, 230° to 140°; Sector II, 140° to 50°; Sector III, 50° through 0° to 320°; and Sector IV, 320° to 230°. During optical eclipse by the moon the sectoring is maintained by an artificial "see-sun" pulse. However, due to thermal shrinkage in the spacecraft and a consequent spin-

up, there is a progressive slippage of the sector pattern relative to the spacecraft-sun line. Data from these periods have been excluded because of the tedium of the correction procedure.

All channels of the solid state detector have an inverse unidirectional geometric factor of 12.7 $(cm^2\ sr)^{-1}$. There is an onboard radioactive alpha particle source that gives continuous background counting rates to assure the proper operation of the detector. These background counting rates have been subtracted prior to all calculations. The P1 and P2 background counting rates are, respectively, 0.0705 and 0.0506 counts/second.

At periapse the moon blocks a significant portion of the detector's field of view, thus reducing the proton flux from that direction [Van Allen and Ness, 1969]. In averages, however, and especially in averages of several hours or more, the moon, due to its rapid angular motion relative to the spacecraft, blocks a particular portion of the sectoring diagram for only a fraction of the averaging period, thus reducing its effect on the directional information of the solar protons to a small value, which is barely significant in the data presented in this work. In half hour data there are occasional periods of otherwise very steady counting rates when lunar shadowing causes an observable modulation.

For the study of solar protons in the interplanetary medium, the data are assumed free of magnetospheric effects when the

spacecraft is located outside of the average magnetoshock location as observed and reported by Behannon [1968].

One-half hour averages of the counting rates of the proton detector channels are used as the base of all data analysis in this paper.

DATA ANALYSIS

A least squares fit to the half-hour counting rates of the four directional sectors of channel P1 is made to an anisotropy model with a unidirectional particle flux of the form:

$$j(\varphi) = A[1 - C \cos(\varphi - \delta)], \qquad (1)$$

where A is the spin averaged value of j; C is the magnitude of the anisotropy; φ is the longitude of the detector's axis in spacecraft centered solar ecliptic coordinates; δ is equal to $\varphi_{max} + 180°$ or $\varphi_{max} - 180°$, whichever is positive and less than 360°; and φ_{max} is the value of φ for which j is a maximum. The angles φ and δ are measured from the spacecraft-sun line in the counterclockwise sense as viewed from the north ecliptic pole. φ_{max} specifies the direction in which the detector is looking at maximum counting rate; δ specifies the spacecraft centered longitude <u>toward</u> which the maximum particle intensity is directed. Note that

$$C = \frac{j_{max} - j_{min}}{j_{max} + j_{min}} .$$

For each set of parameters, the observed anisotropy vector is defined as the vector (C, δ). It is, of course, only the projection on the ecliptic plane of the full, three-dimensional anisotropy vector.

An exemplary case of actual data for the half-hour period 0130-0200 UT of August 11, 1967 is as follows:

Sector I	226.8 counts/sec
Sector II	220.5
Sector III	441.1
Sector IV	427.2

From these data:

$$A = 328.8 \text{ counts/sec} = 4176 \text{ (cm}^2 \text{ sec sr)}^{-1}$$
$$C = 0.503$$
$$\varphi_{max} = 320°$$
$$\delta = 140°$$

The limitations of equation (1) are recognized but the nature of the basic angular distribution data does not appear to justify a more elaborate analysis.

Anisotropy vectors for periods of greater than a half-hour are found by taking the separate means of the two cartesian components of each of the half hour vectors included. The result is then re-expressed as a polar vector.

Since P1 and P2 detect protons over different energy ranges, the ratio P1/P2 gives information on the form of the proton energy distribution. Inasmuch as the relevant spectral quantity in the present investigation is the logarithmic derivative

$$\frac{d\left[\ell n\left(\frac{dj}{dE}\right)\right]}{d\left[\ell n\ E\right]},$$

where E is kinetic energy, a power law differential spectrum of the simple form

$$\frac{dj}{dE} = K\ E^{\gamma} \qquad (2)$$

has been adopted as adequate over the limited energy range of importance (0.3 to several MeV). Because the energy ranges of P1 and P2 are nested, there are in general two possible values of γ corresponding to a given P1/P2 ratio, one greater than -1.39 and one less than -1.39. Conclusive resolution of this ambiguity has been accomplished in a number of cases by use of simultaneous polar cap data from the earth-orbiting satellite Injun 5. (See later section.)

Two different graphical representations of the anisotropy data are used in this study. The first is a direct plot of the anisotropy and spectral parameters A, C, δ, and γ versus time [Figures 8-14]. The error bars on all quantities are omitted when they are of the order of the point size. When the counting rates are low, or when both values of γ are approximately -1.39, the calculated uncertainty in the ratio P1/P2 may show that the

uncertainties in both values are larger than the difference between the two values. Then both points are shown on a single combined error bar. Along the top border of the plots there are several symbols which indicate the location of the spacecraft. The triangles indicate the times of periapse, a solid line indicates that the spacecraft is within the average boundaries of the magnetotail, and a dashed line indicates that the spacecraft is outside of the magnetotail but behind the average location of the earth's bow shock [Behannon, 1968].

The second useful representation of the proton anisotropy data is the "anisotropy vector sum" plot. Such a plot is produced by arranging successive anisotropy vectors "head to tail" to show the time dependence of the anisotropy vector [Figures 1-7] In the plots given here, the anisotropy vectors are six hour averages. Also the average orientation (i.e., ignoring the vector sense) of the interplanetary magnetic field is shown for each anisotropy vector by a light line through its tail. Alpha is the angle between the anisotropy vector and the magnetic field line.

Other data used in this paper include one-hour magnetic field averages from Explorer 35 kindly supplied by K. W. Behannon and N. F. Ness of the Goddard Space Flight Center and by D. S. Colburn of the Ames Research Center. The solar wind data are from the Vela satellites of the Los Alamos Scientific Laboratory as published

in Solar Geophysical Data 1969 through 1970. During the years 1969 and 1970 the maximum reported solar wind velocity was 770 km/sec on January 26, 1969 and the minimum was 234 km/sec on June 23, 1970.

NET FLUX OF PROTONS $E_p > 0.3$ MeV

Using the parameters A, C, and δ from the fitting of equation (1) to observed data, the net flux of protons, f, through a unit area perpendicular to the spacecraft-sun line is given by

$$f = 12.7 \int_0^{2\pi} A\,[1 - C \cos(\varphi - \delta)] \cos\varphi \, d\varphi$$

or

$$f = -12.7\,\pi\,A\,C \cos\delta \quad . \tag{3}$$

The quantity f is positive (net flux outward from the sun) for $90° < \delta < 270°$ and negative (net flux inward toward the sun) for $0° < \delta < 90°$ and $270° < \delta < 360°$. It is conveniently measured in $(cm^2\ sec)^{-1}$. The time integral of f over a particular solar particle event gives the total number of particles per unit area flowing past the spacecraft for that event. The result has been expressed as the number of particles per unit solid angle at 1 AU referenced to the sun as the apex of the infinitesimal solid angle. No

implications of rectilinear propagation or of isotropic emission at the sun are intended by this convention.

Table 1 gives N, the number of protons $E_p > 0.3$ MeV per steradian flowing past the spacecraft during the course of the event, for those "simple" events under study by observations essentially clear of the magnetosphere. "Simple" events are those whose time history suggests that they are attributable to a single solar flare. They are characterized, generally, by a rise phase of 1 to 2 days duration and a decay phase of 3 to 8 days duration. The intensity-time curves are grossly, but not accurately, monotonic during the respective phases.

Solar particle events are identified with particular flares by comparing the onset times of high energy protons, prompt energetic electrons, and solar X rays (all of which are available from the University of Iowa experiment on Explorer 35) to the onset time of optical flares as tabulated in Solar-Geophysical Data of the U. S. Department of Commerce. Usually one flare can be identified with reasonable certainty as being the parent flare for an event. An exception is the event of May 13, 1969 which had a very gradual onset in both high energy protons and energetic electrons, and no discernible X-ray emission. The only flares occurring near the presumed time of particle emission were sub-flares. Thus it appears reasonably certain that this event must be attributed to a flare on the invisible hemisphere of the sun.

Several conclusions can be drawn from the information in Table 1. First there is a clear positive correlation between the maximum intensity of an event and N. This non-surprising result simply means that the form of intensity-time curves is more or less independent of the "size" of the event. Table 2 shows the average value of N for three ranges of maximum intensity in the events. Because the number of events clear of the magnetosphere is small, the results in Table 2 can not be taken, however, as thoroughly definitive.

Another observation from Table 1 concerns the relationship of N to the solar longitude of the parent flare. If the dominant mode of transport for 0.3 MeV solar protons were convective with little or no diffusion either along or across the interplanetary magnetic field lines, one would expect the flare longitudes to be clustered around 0°. If the dominant transport mechanism were fast diffusion along field lines, with little or no convection and slow cross field diffusion (the case for higher energy protons), then one would expect to find the largest events from flares around west 50° solar longitude (where the interplanetary magnetic field lines through the earth reach the sun). Mixing the convective and parallel field diffusive transport mechanisms would give an optimal flare longitude between these extremes. An increasingly important degree of cross field diffusion would tend to smear this distribution.

Despite the small number of events in Table 1, and the statistical inadequacy of the body of data, it is of interest that the events with the largest N values are clustered around or somewhat to the east of 0° solar longitude. The one exception to this is the November 18, 1968 event, which was caused by a western limb flare, and which, judging from the particle data, was by far the largest simple event of those under study. If a similar clustering around 0° solar longitude were observed for an adequately large number of events, this evidence alone would suggest radial convection as the dominant transport mechanism for protons $E_p \geq 0.3$ MeV.

THE DIFFUSIVE AND CONVECTIVE COMPONENTS OF THE ANISOTROPY

Figures 1 through 7 show anisotropy vector sum plots for the seven largest events of those being studied. The vectors are six hour averages in all cases. Figures 8 through 14 show the A, C, δ, and γ versus time plots for the same seven events. Several common characteristics are seen in these data. During the rise phase of each event the anisotropy vector tends to align itself with the interplanetary magnetic field more closely than it does later in the event. During the rise phases of all but the June 25, 1970 event (Figure 7) α, the angle between the field line and the anisotropy vector, tends to be negative, that is, the anisotropy vector, while being nearly in the same direction as the interplanetary field lines, lies between the field line orientation and the outward radial direction. During the decay phases the anisotropy tends to be more nearly radially outward and less dependent on the field direction. These observations are in qualitative agreement with those by McCracken et al. [1968] for 7.5 to 45 MeV solar protons.

The above results support the hypotheses (a) that in the early portion of a solar proton event the dominant particle

transport mechanism is diffusive, with the diffusion tensor such that diffusion takes place primarily along the magnetic field lines and (b) that later in the event the anisotropy is mainly attributable to radially outward convection by the solar wind.

The matter has been discussed in convenient theoretical form by Forman [1970a] [1970b]. There she divides the theoretical anisotropy vector Δ into two components: Δ_d, the diffusive component, and Δ_c, the convective component. The diffusive component of the anisotropy vector is determined by the gradient in the particle density U and the diffusion tensor K:

$$\Delta_d = -\frac{3}{v} \cdot \frac{K \cdot \nabla U}{U} \tag{4}$$

where v is the particle velocity. The convective component is the kinematic anisotropy which results from transforming any assumed distribution in the rest frame of the solar wind to the observer's frame of reference (Compton-Getting effect). For an infinitesimal portion of a continuous particle spectrum at kinetic energy E and velocity v the theoretical value of the convective component of the anisotropy vector is

$$\Delta_c = \left\{ 2 - \alpha \frac{d\left[\ell n \left(\frac{dj}{dE}\right)\right]}{d[\ell nE]} \right\} \frac{V}{v} \tag{5}$$

where V is the convection or solar wind velocity, $\alpha = 2$ for 0.3 MeV protons, and dj/dE is the differential energy spectrum of the particles at energy E. For the adopted spectral form of equation (2), equation (5) becomes:

$$\Delta_c = (2 - 2\gamma)\ V \left\langle \frac{1}{v} \right\rangle \qquad (6)$$

where $\left\langle \frac{1}{v} \right\rangle$ is the spectral average of the reciprocal particle velocity over the energy range of the detector. Assuming that K is such that diffusion along the field predominates over cross field diffusion, Δ_d will be along the field line and Δ_c will be radially outward.

In view of the above theoretical guidance the observed anisotropy vector (C, δ) is resolved into two components: a radial component with magnitude C_R, and a field aligned component with magnitude C_M (see Figure 15). The magnitude of the components is considered positive outward from the sun. The identification of C_R with Δ_c and C_M with the diffusive anisotropy Δ_c is valid only insofar as field aligned diffusion dominates cross field diffusion.

Figures 16 through 22 show C_M and C_R for the seven above mentioned events. The values are six hour averages of one hour C_R and C_M data. The error bars show the statistical standard deviations of the one hour data from the mean value during the six hour period. In periods of low counting rate, because of poor

statistics, sometimes not all six values are included in the average, thus causing the standard deviation to possibly be an underestimation of the scatter. When the interplanetary magnetic field approaches the radial direction, the resolution of the anisotropy vector into C_R and C_m becomes indeterminate. Thus, in cases when the field is within 10° of the radial direction, resolution of the anisotropy vector has not been attempted.

The significance of C_R is examined with the help of equation (6) for the theoretical value of Δ_c, the convective component of the anisotropy. As remarked earlier and as shown explicitly in Figures 8-14, two different values of the spectral parameter γ are found, in general, for any observed ratio P1/P2. Hence, two, usually quite different, values of Δ_c are found by equation (6).

To resolve this ambiguity a comparison of Explorer 35 spectral data was made with spectral data in a similar energy range obtained from simultaneous observations of solar protons over the polar caps of the earth with the University of Iowa satellite Injun 5. An unambiguous value for γ was obtained from the ratio of the counting rates of the $0.3 \leq E_p \leq 9.2$ MeV channel to the $0.3 \leq E_p \leq 1.4$ MeV channel of the solid state detector of Injun 5. This comparison was possible for the following periods of those under study: decimal days 24.0 to 26.0, 1969; days

80.0 to 85.0, 1969; days 134.0 to 136.0, 1969; and days 32.0 to 34.0 1970 (decimal day 0.5 being 1200 UT January 1). In these four cases, all of some 36 Injun 5 values of γ, without exception, were accurately consistent with the $\gamma < -1.39$ branch of the ambiguous Explorer 35 curve of P1/P2 vs γ and were clearly inconsistent with the $\gamma > -1.39$ branch. On the basis of this evidence for four specific events. it is concluded tentatively that the more negative value of γ is the proper choice for all of the events under study here.

Hence, a unique value of Δ_c is found by equation (6), using Vela values of V whenever such data are available. These theoretical values of Δ_c are shown as open squares in Figures 18-22 for comparison with the observed values of C_R.

In the decay phases of all events for which this comparison has been possible, there is excellent agreement between Δ_c and C_R, thus supporting the hypothesis that the radial component of the anisotropy in the decay phase of a solar proton event is attributable to the convection of protons by frozen-in magnetic irregularities in the solar wind.

Further, during the rise phase of most events, C_R behaves in a corresponding manner; that is, it is positive and relatively constant in magnitude at a value consistent with usual values of V, even though observed values of V are somewhat sparse. An exception seems to be the rise phase of the event of June 25, 1970 (Figure 22).

Here C_M is strongly positive early in the event. At corresponding times C_R is strongly negative; later C_R becomes zero then goes positive and remains approximately constant at ~ 0.4 during the decay phase as C_M tends toward zero and then toward negative values. No explanation for this case is offered, though it is clear also from Figure 7 that this is an unusual event.

Insofar as the above evidence justifies the identification of C_R with the theoretical convective anisotropy Δ_c in the decay phase of simple solar events, and, in some cases, also in the rise phase, then, by elimination, C_M must be the diffusive contribution to the anisotropy during these periods. Making this identification, we can draw some inferences about the particle density gradient using equation (4).

For the events of November 18, 1968 (Figure 17), March 21, 1969 (Figure 19), January 31, 1970 (Figure 21), and June 25, 1970 (Figure 22) C_M is negative for a significant portion, if not most, of the decay phase. This is taken to mean that there is a positive radial gradient in the particle density U (i.e., U increases with increasing heliocentric distance), thus causing a sunward diffusion of protons. Since the particles were injected initially at the sun, it appears that the positive gradient must have been caused by the bulk convective transport of particles outward by the solar wind [cf. McCracken et al., 1971]. This observation gives striking evidence for the importance of convection at these energies.

A typical value of C_M during these positive gradient periods is about -0.2, which gives, by equation (4), a value for $K \cdot \nabla U/U$ of about 7×10^{20} cm^2/sec - AU.

In those rise phase cases where C_R can be identified with the theoretical convective anisotropy, such as in the August 9, 1967 event (Figure 16) and the March 21, 1969 event (Figure 19), the behavior of C_M is qualitatively what one would expect of the diffusive component of the anisotropy, namely, C_M decays from a high positive initial value to the decay phase values over a period of one or two days. A typical initial rise phase value for C_M of +1.0 corresponds to a negative radial gradient in the particle density with $K \cdot \nabla U/U$ of about -3×10^{21} cm^2/sec - AU. Since both of these cases are from eastern flares, the fact that protons are diffusing down magnetic field lines near the earth that lead to the western side of the sun indicates that protons $E_p \geq 0.3$ MeV are injected into, or diffuse into, a region interior to the earth's orbit that is very broad in solar longitude.

McCracken et al. [1968] have reported the effects of interplanetary magnetic field reversals on 7.5 MeV solar protons. The observed effects on 0.3 MeV solar protons for the periods under study here are variable. During the March 21, 1969 event there is a single magnetic field reversal (Figure 4) which, while having observable effects on A, C, and δ (Figure 11), had no effect on C_R and did not interrupt the decay of C_M (Figure 19).

In the May 13, 1969 event there was a series of field reversals and irregularities. In this event C_M (Figure 20) remained positive and relatively constant indicating that protons were diffusing outward from the sun for the entire event despite the field reversals. In the January 31, 1970 event there were many interplanetary magnetic field irregularities. As seen in Figure 21, C_M in the decay phase of this event was negative, indicating diffusion inward along the field lines toward the sun.

ACKNOWLEDGEMENTS

This paper is based on the Ph.D. dissertation of the first author [Innanen, 1972], wherein a considerably larger body of data and additional details are given. The solid state detector on the NASA/GSFC satellite Explorer 35 was developed at the University of Iowa by Drs. S. M. Krimigis and T. P. Armstrong. Interplanetary magnetic field data from the two magnetometers on Explorer 35 were kindly supplied by Drs. K. W. Behannon and N. F. Ness of the Goddard Space Flight Center and Dr. D. S. Colburn of the Ames Research Center. The data on the solar wind velocities were taken from Los Alamos Scientific Laboratory observations with the Vela satellites as published in Solar-Geophysical Data of the U. S. Department of Commerce.

One of us (W.G.I.) is grateful for a NASA predoctoral traineeship 1965-68.

The hardware phase of this work was supported by contract NAS5-9076 with the Goddard Space Flight Center. Analytical work has been supported by contract N00014-68-A-0196-0003 with the U. S. Office of Naval Research.

REFERENCES

Behannon, K. W., Mapping of the earth's bow shock and magnetic tail by Explorer 33, J. Geophys. Res., 73, 907-930, 1968.

Forman, M. A., The Compton-Getting effect for cosmic-ray particles and photons and the Lorentz-invariance of distribution functions, Planet. Space Sci., 18, 25-31, 1970a.

Forman, M. A., The equilibrium anisotropy in the flux of 10-MeV solar particles and their convection in the solar wind, J. Geophys. Res., 75, 3147-3153, 1970b.

Innanen, W. G., Anisotropies in 0.3 MeV solar protons, Ph.D. dissertation, University of Iowa, May 1972.

McCracken, K. C., U. R. Rao, R. P. Bukata, and E. P. Keath, The decay phase of solar flare events, Solar Phys., 18, 100-132, 1971.

McCracken, K. C., U. R. Rao, and N. F. Ness, Interrelationship of cosmic-ray anisotropies and the interplanetary magnetic field, J. Geophys. Res., 73, 4159-4166, 1968.

Pieper, G. F., A. J. Zmuda, C. O. Bostrom, and B. J. O'Brien, Solar protons and magnetic storms in July 1961, J. Geophys. Res., 67, 4959-4981, 1962.

Van Allen, J. A., and L. A. Frank, Mariner II. The Iowa radiation experiment, Science, 138, 1097-1098, 1962.

Van Allen, J. A., L. A. Frank, and D. Venkatesan, Trans., Am. Geophys. Union, 45, 80, 1964 (Abstract P27).

Van Allen, J. A., and N. F. Ness, Particle shadowing by the moon, J. Geophys. Res., 74, 71-93, 1969.

Table 1

A Table of N for Simple Events Clear of the Magnetosphere

(See Text)

Event of	Decimal Days From	To	N (protons/sr)	Maximum Intensity (c/s)	Flare Longitude	Flare Importance
Nov. 18, 1968	322.50	333.00	1.6×10^{35}	1.8×10^{3}	W 70°	1B**
Aug. 9, 1967	220.75	226.00	9.8×10^{34}	5.3×10^{2}	E 32°	2B
May 13, 1969	132.75	140.00	9.4×10^{34}	1.3×10^{3}	***	***
Jan. 24, 1969	23.33	30.00	8.6×10^{34}	2.2×10^{2}	W 09°	2B
Mar. 21, 1969	79.00	88.00	5.5×10^{34}	3.0×10^{2}	E 16°	2N
June 25, 1970	175.50	181.00	4.3×10^{34}	9.2×10^{2}	E 11°	2B
Jan. 31, 1970	30.75	36.00	1.6×10^{34}	1.9×10^{2}	W 62°	2B
July 1, 1970	181.00	186.75	9.8×10^{33}	1.0×10^{2}	E 83°	1F
Nov. 27, 1967	330.00	336.25	5.9×10^{33}	7.0×10^{1}	W 41°	1F
July 6, 1970	186.75	192.00	5.1×10^{33}	2.5×10^{1}	W 90°	1B**

**West limb flare

***Subflares only

Table 2

A Table of N for Several Ranges of Maximum Intensity for Simple Events Clear of the Magnetosphere

Maximum Intensity Range (c/s)	Average N (protons/sr)	Number of Events
$I > 9 \times 10^2$	9.8×10^{34}	3
$10^2 < I < 9 \times 10^2$	3.9×10^{34}	5
$10^1 < I < 10^2$	5.5×10^{33}	2

FIGURE CAPTIONS

Figure 1. Anisotropy vector sum plot (six-hour averages) for the event of August 9, 1967. The X_{SE} Y_{SE} Z_{SE} coordinate system is a spacecraft centered one with the X_{SE} Y_{SE} plane parallel to the ecliptic, the $+X_{SE}$ axis toward the sun, and the $+Z_{SE}$ axis toward the north ecliptic pole.

Figure 2. Anisotropy vector sum plot (six-hour averages) for the event of November 18, 1968.

Figure 3. Anisotropy vector sum plot (six-hour averages) for the event of January 24, 1969.

Figure 4. Anisotropy vector sum plot (six-hour averages) for the event of March 21, 1969.

Figure 5. Anisotropy vector sum plot (six-hour averages) for the event of May 13, 1969.

Figure 6. Anisotropy vector sum plot (six-hour averages) for the event of January 31, 1970.

Figure 7. Anisotropy vector sum plot (six-hour averages) for the event of June 25, 1970.

Figure 8. Anisotropy parameters and indices of a power law energy spectrum (see text) for the period decimal days 220.0 through 226.0, 1967 (decimal day 220.0 =

August 9 on 0000 UT). The parent flare occurred on decimal day 220 at 1815 UT.

Figure 9. Anisotropy parameters and indices of a power law energy spectrum (see text) for the period decimal days 322.0 through 333.0, 1968 (decimal day 322.0 = November 18 at 0000 UT). The parent flare occurred on decimal day 322 at 1017 UT.

Figure 10. Anisotropy parameters and indices of a power law energy spectrum (see text) for the period decimal days 23.0 through 31.0, 1969 (decimal day 23.0 = January 24 at 0000 UT). The parent flare occurred on decimal day 23 at 0803 UT.

Figure 11. Anisotropy parameters and indices of a power law energy spectrum (see text) for the period decimal days 79.0 through 88.0, 1969 (decimal day 79.0 = March 21 at 0000 UT). The parent flare occurred on decimal day 79 at 0141 UT.

Figure 12. Anisotropy parameters and indices of a power law energy spectrum (see text) for the period decimal days 132.0 through 140.0, 1969 (decimal day 132.0 = May 13 at 0000 UT). No major flares preceded the onset of the event.

Figure 13. Anisotropy parameters and indices of a power law energy spectrum (see text) for the period decimal days 30.0 through 36.0, 1970 (decimal day 30.0 = January 31 at 0000 UT). The parent flare occurred on decimal day 30 at 1512 UT.

Figure 14. Anisotropy parameters and indices of a power law energy spectrum (see text) for the period decimal days 175.0 through 181.0, 1970 (decimal day 175.0 = June 25 at 0000 UT). The parent flare occurred on decimal day 175 at 1833 UT.

Figure 15. An illustration of the resolution of the observed anisotropy vector C into a radial component C_R and a component C_M along the local magnetic field line BB'. The diagram is in the ecliptic plane. The sense of the magnetic vector is ignored.

Figure 16. The anisotropy components C_M and C_R for the event of August 9, 1967.

Figure 17. The anisotropy components C_M and C_R for the event of November 18, 1968.

Figure 18. The anisotropy components C_M and C_R for the event of January 24, 1969. The open squares are calculated values of Δ_c.

Figure 19. The anisotropy components C_M and C_R for the event of March 21, 1969. The open squares are calculated values of Δ_c.

Figure 20. The anisotropy components C_M and C_R for the event of May 13, 1969. The open squares are calculated values of Δ_c.

Figure 21. The anisotropy components C_M and C_R for the event of January 31, 1970. The open squares are calculated values of Δ_c.

Figure 22. The anisotropy components C_M and C_R for the event of June 25, 1970. The open squares are calculated values of Δ_c.

B-G71-695

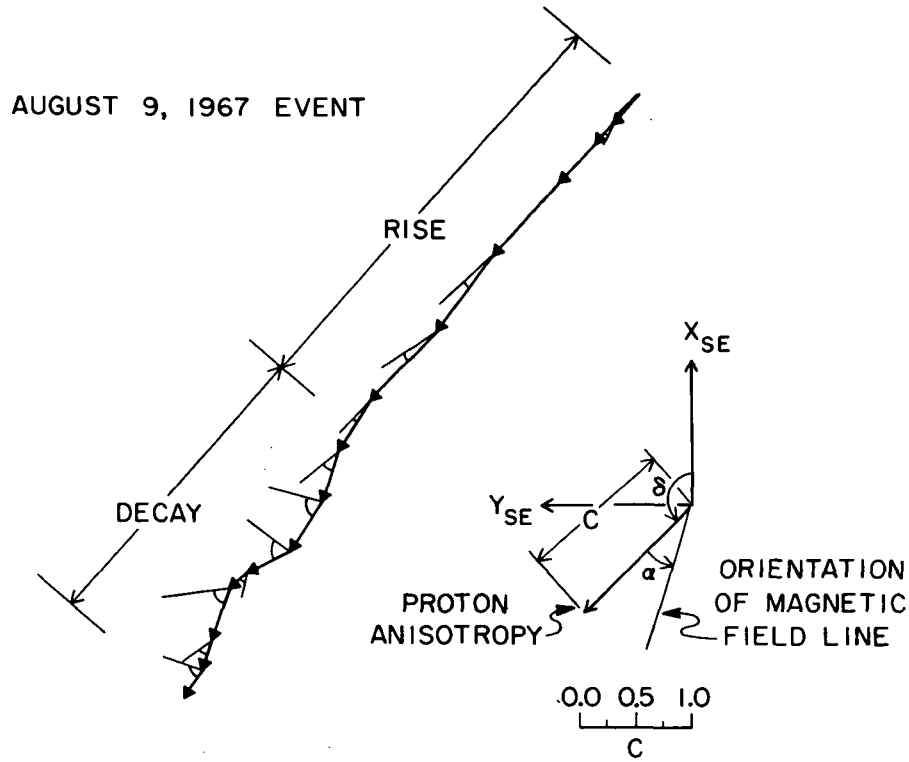

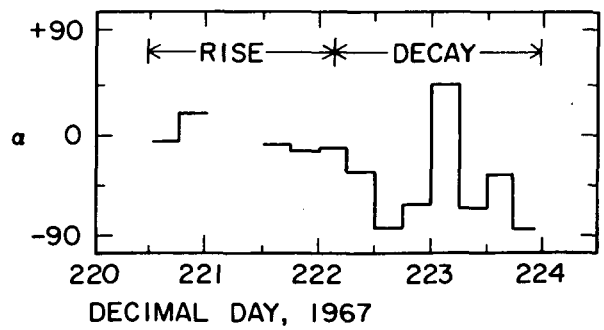

Figure 1

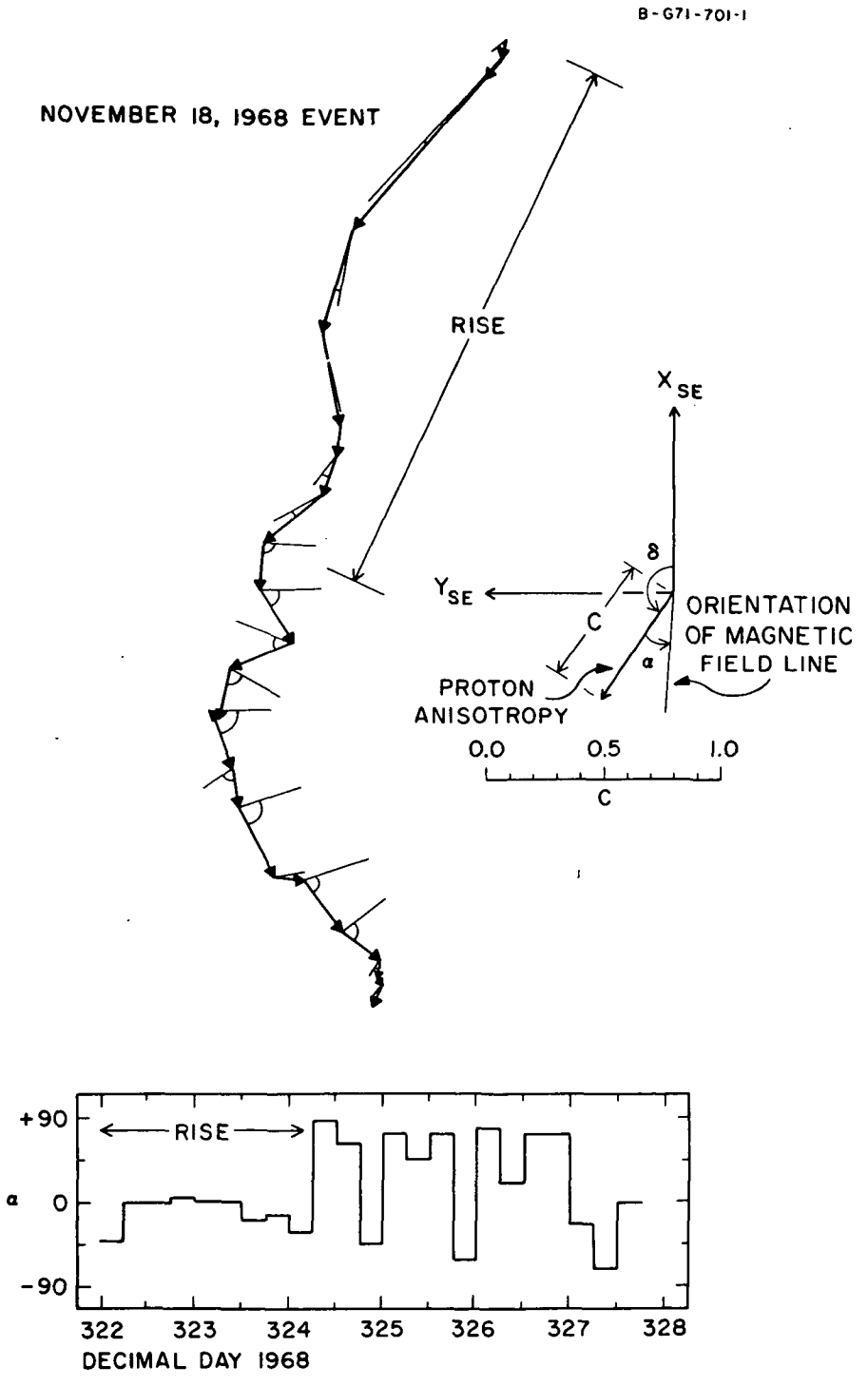
B-G71-701-1
NOVEMBER 18, 1968 EVENT
RISE
X_{SE}
Y_{SE}
δ
C
α
ORIENTATION
OF MAGNETIC
FIELD LINE
PROTON
ANISOTROPY
0.0
0.5
1.0
C
+90
RISE
α
0
-90
322
323
324
325
326
327
328
DECIMAL DAY 1968

Figure 2

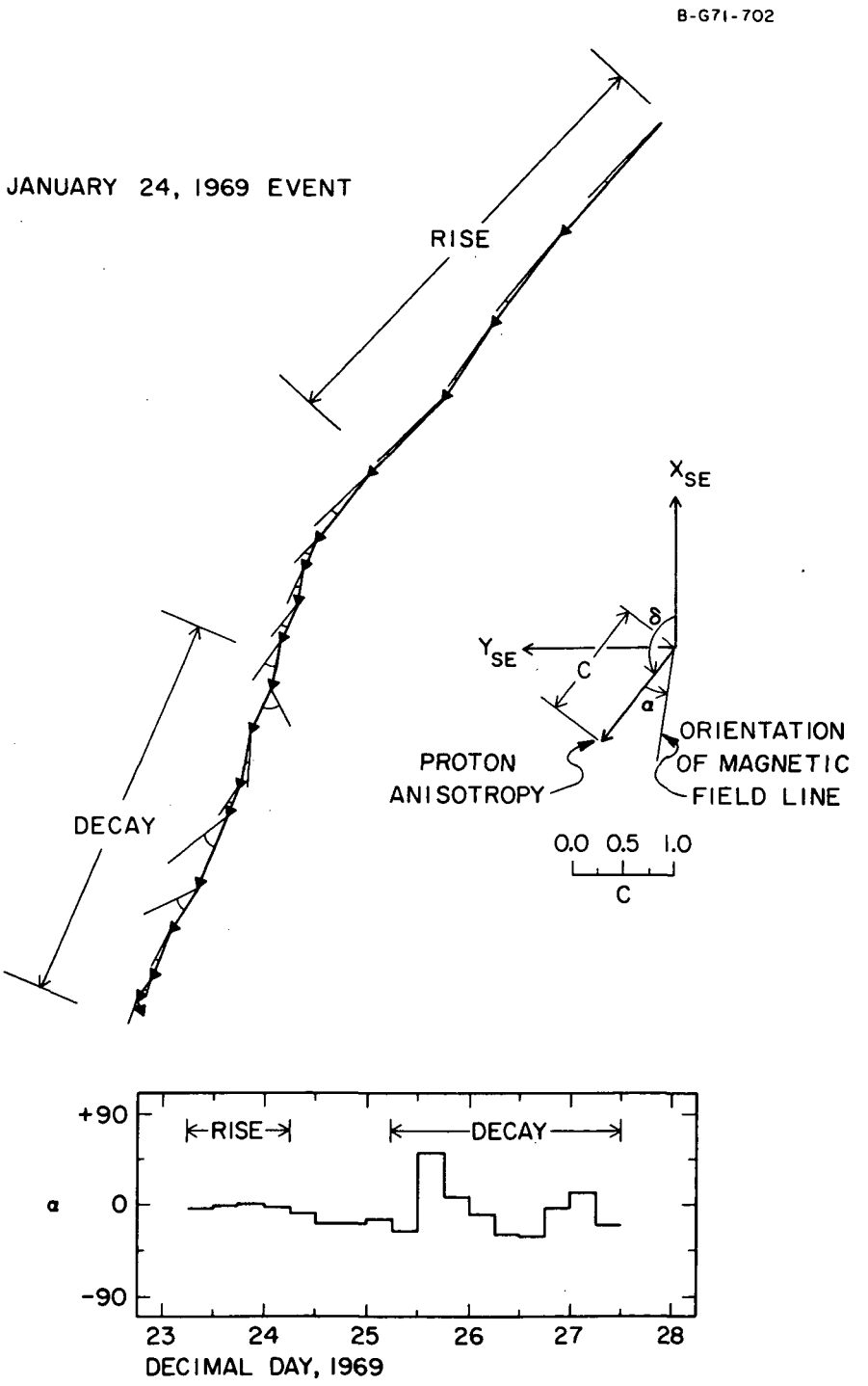
B-G71-702
JANUARY 24, 1969 EVENT
RISE
DECAY
X_{SE}
Y_{SE}
δ
C
α
PROTON ANISOTROPY
ORIENTATION OF MAGNETIC FIELD LINE
0.0 0.5 1.0
C
+90
0
-90
α
RISE
DECAY
23
24
25
26
27
28
DECIMAL DAY, 1969

Figure 3

B-G71-706

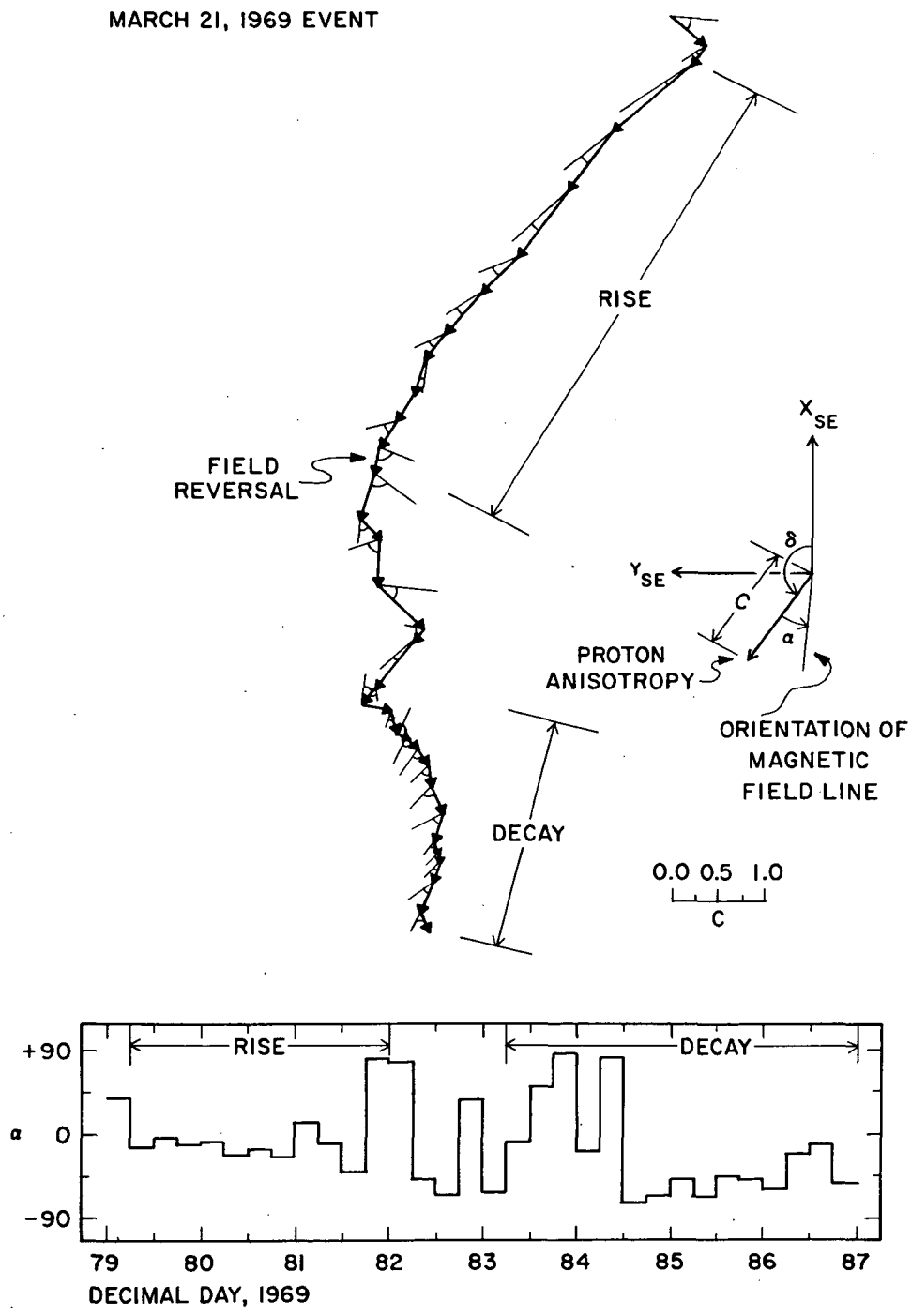

Figure 4

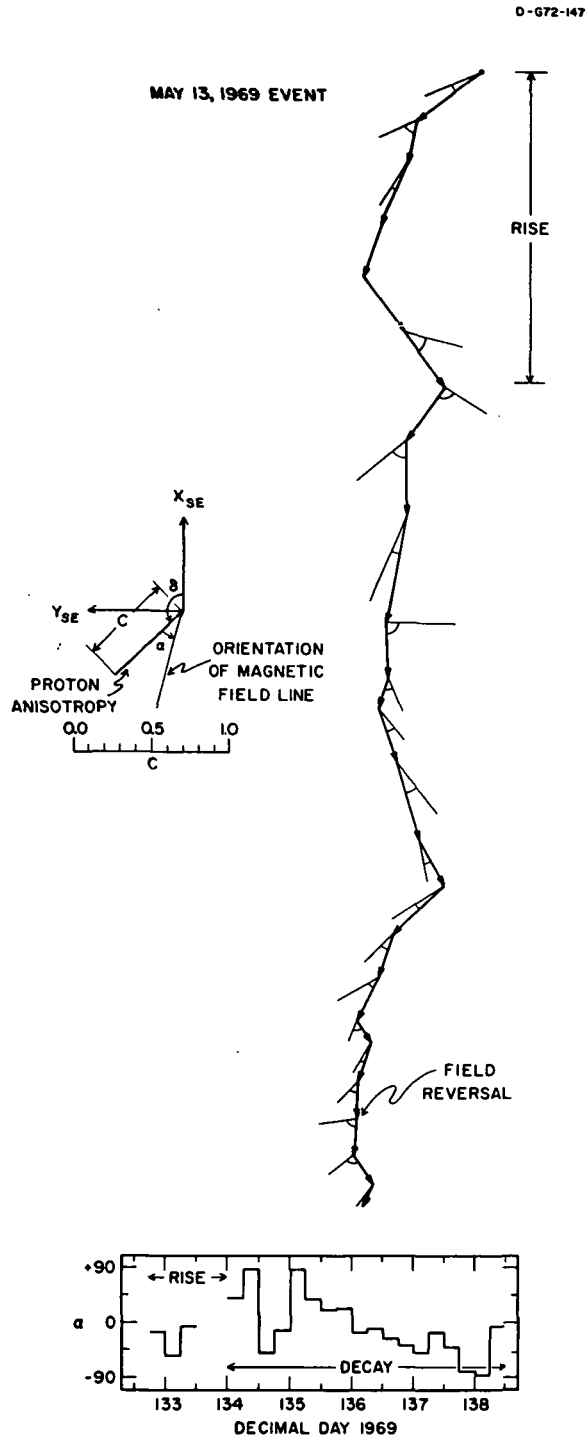
D-G72-147
MAY 13, 1969 EVENT
RISE
X_{SE}
Y_{SE}
β
C
α
ORIENTATION
OF MAGNETIC
FIELD LINE
PROTON
ANISOTROPY
0.0
0.5
1.0
C
FIELD
REVERSAL
+90
α
0
-90
← RISE →
DECAY
133
134
135
136
137
138
DECIMAL DAY 1969

Figure 5

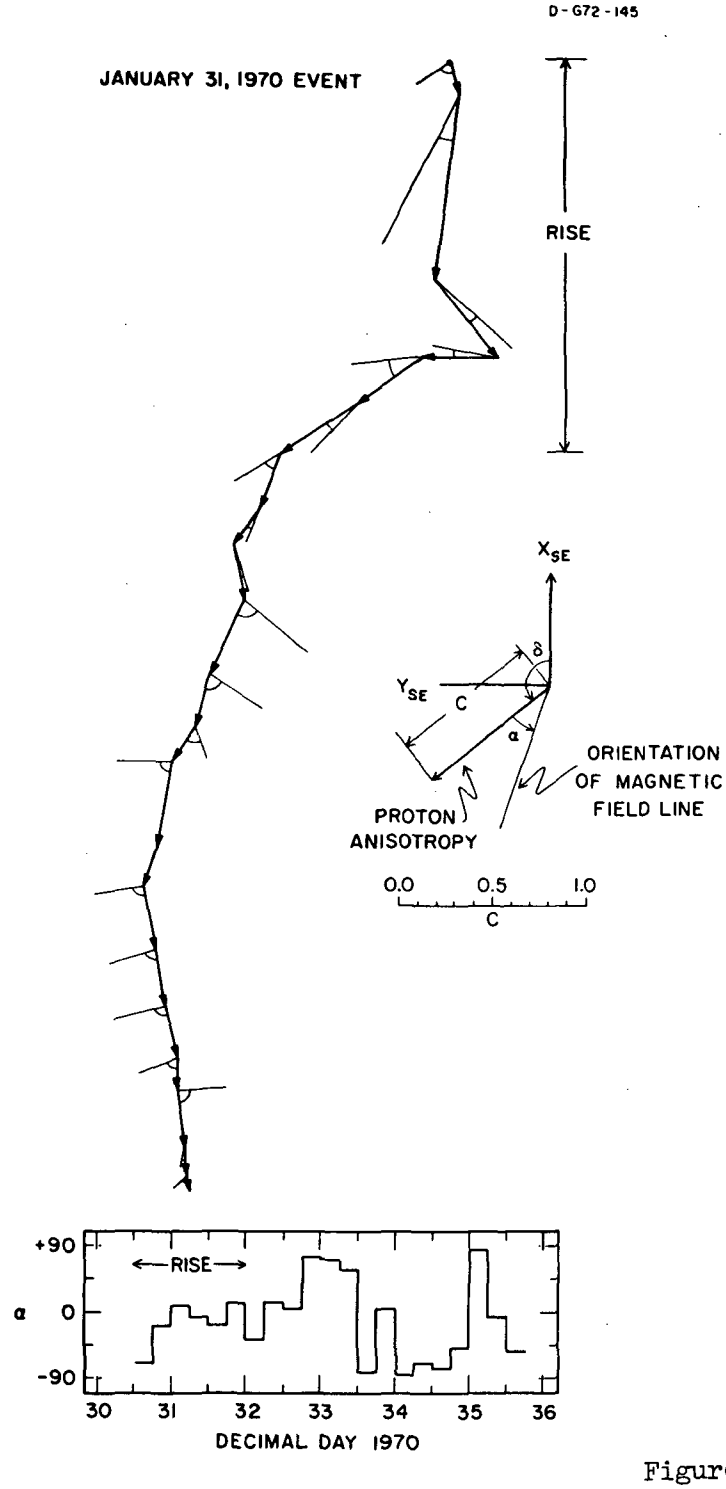
D-G72-145
JANUARY 31, 1970 EVENT
RISE
X_{SE}
Y_{SE}
C
δ
α
ORIENTATION
OF MAGNETIC
FIELD LINE
PROTON
ANISOTROPY
0.0
0.5
1.0
C
+90
α
0
-90
RISE
30
31
32
33
34
35
36
DECIMAL DAY 1970

Figure 6

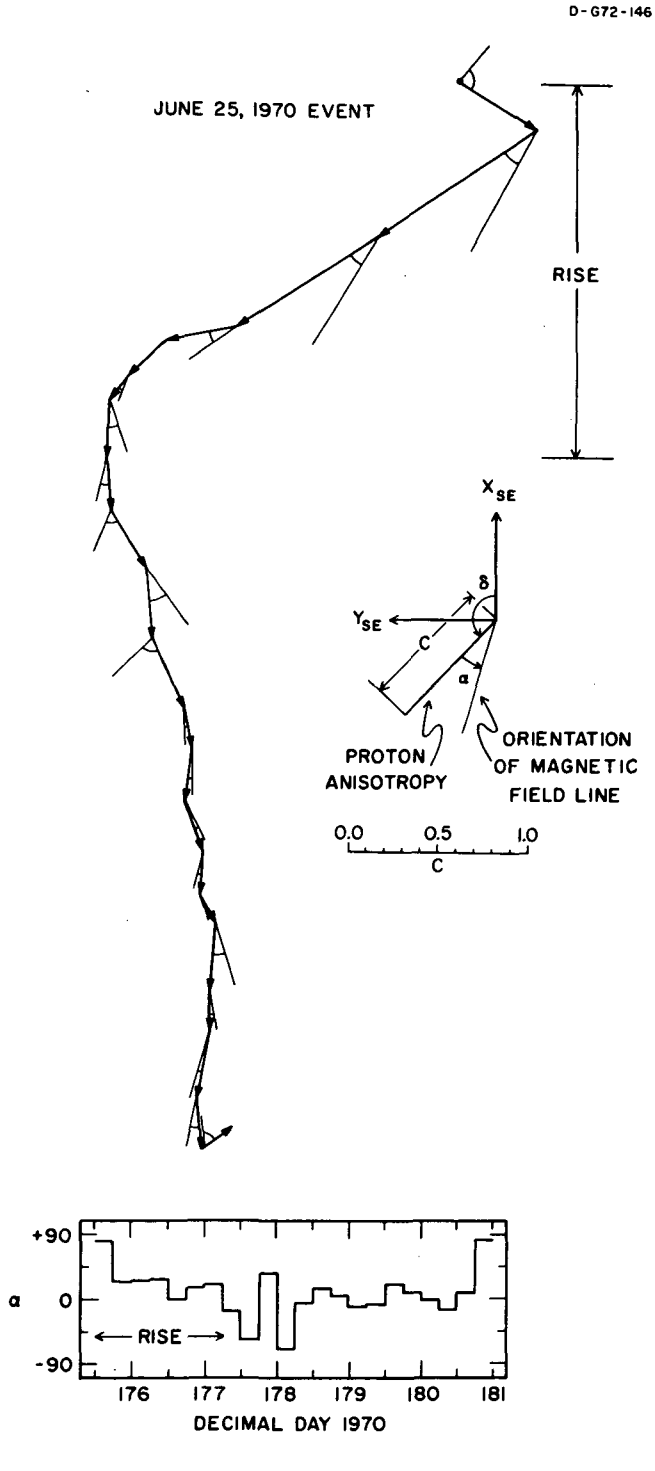
D-G72-146
JUNE 25, 1970 EVENT
RISE
X_{SE}
Y_{SE}
δ
C
α
PROTON ANISOTROPY
ORIENTATION OF MAGNETIC FIELD LINE
0.0
0.5
1.0
C
+90
α
0
-90
RISE
176
177
178
179
180
181
DECIMAL DAY 1970

Figure 7

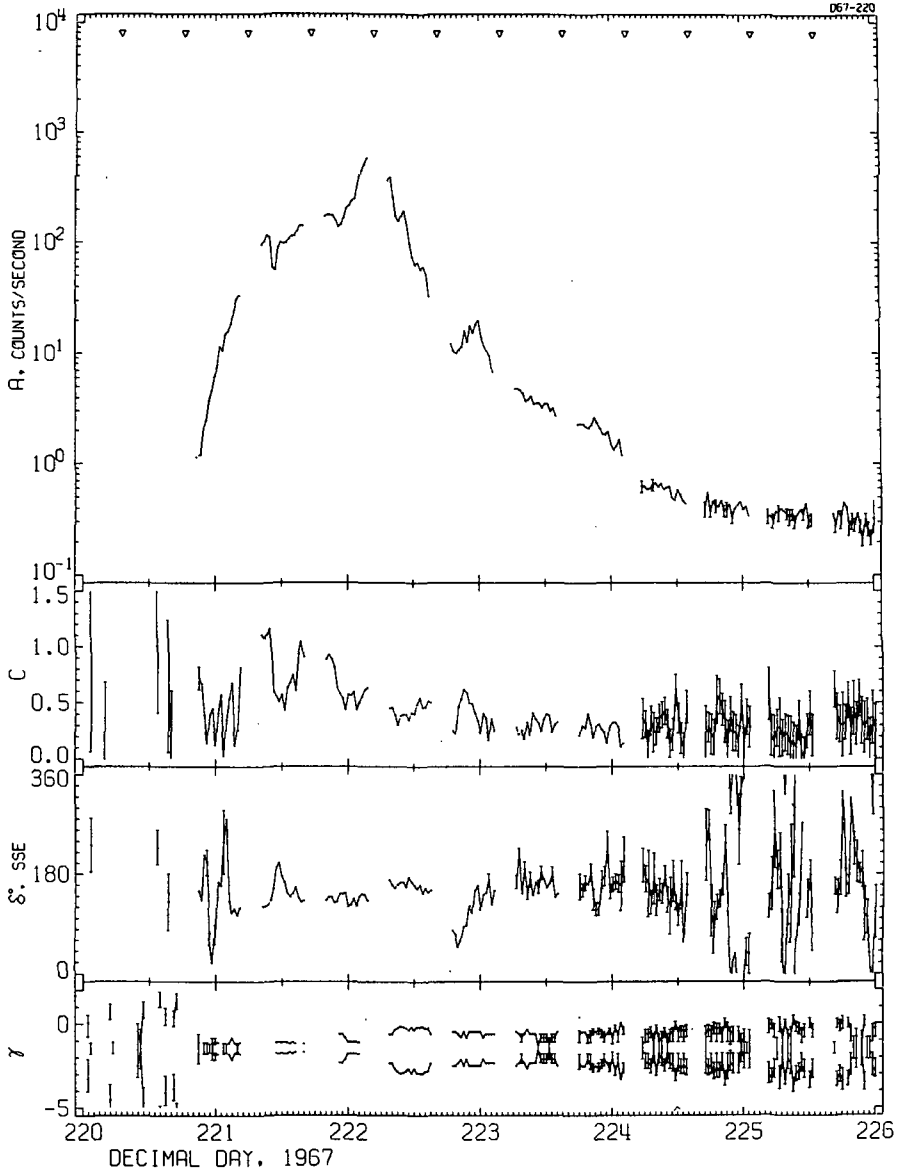
D67-220
A, COUNTS/SECOND
10^4
10^3
10^2
10^1
10^0
10^{-1}
C
1.5
1.0
0.5
0.0
δ°, SSE
360
180
0
γ
0
-5
220
221
222
223
224
225
226
DECIMAL DAY, 1967

Figure 8

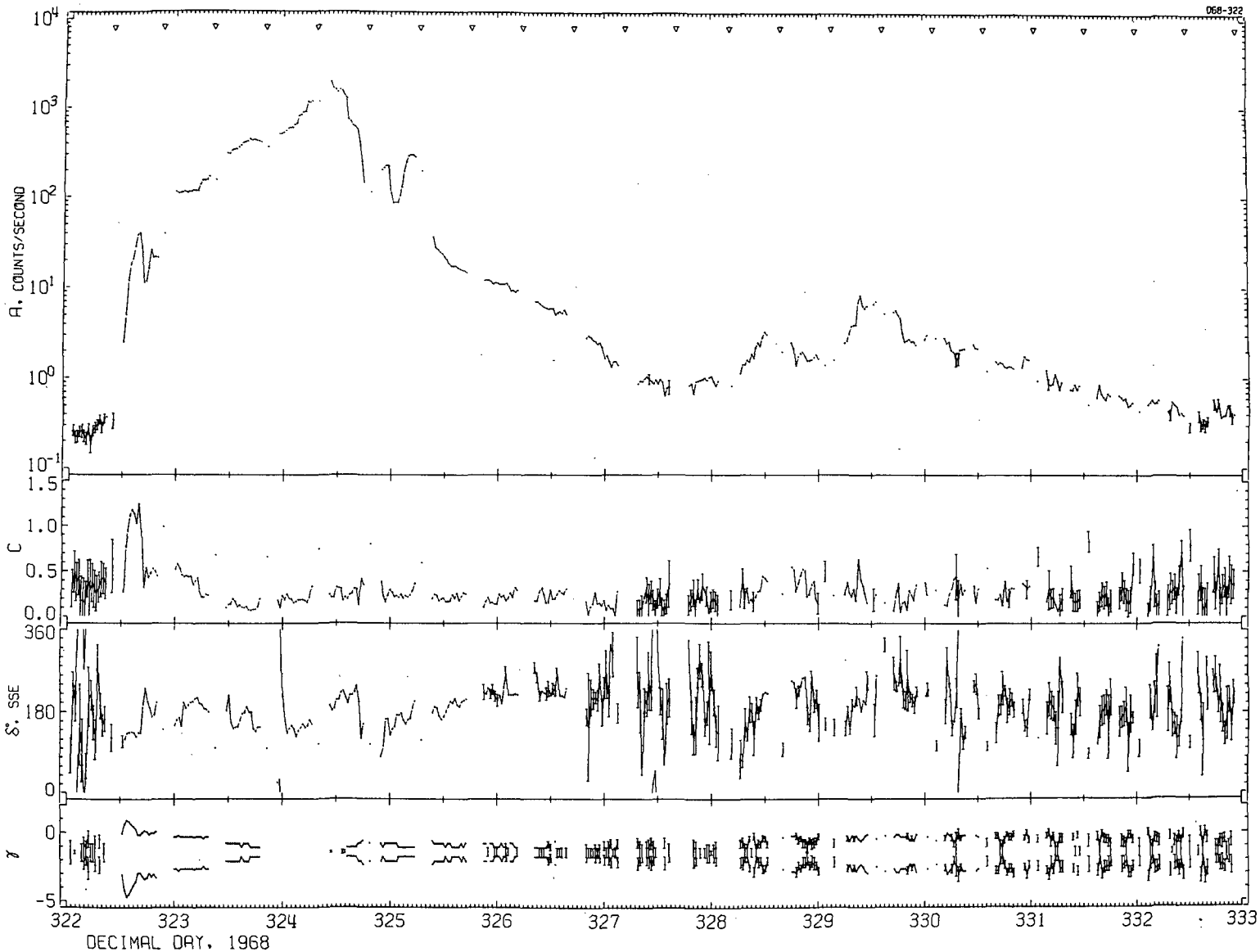

Figure 9

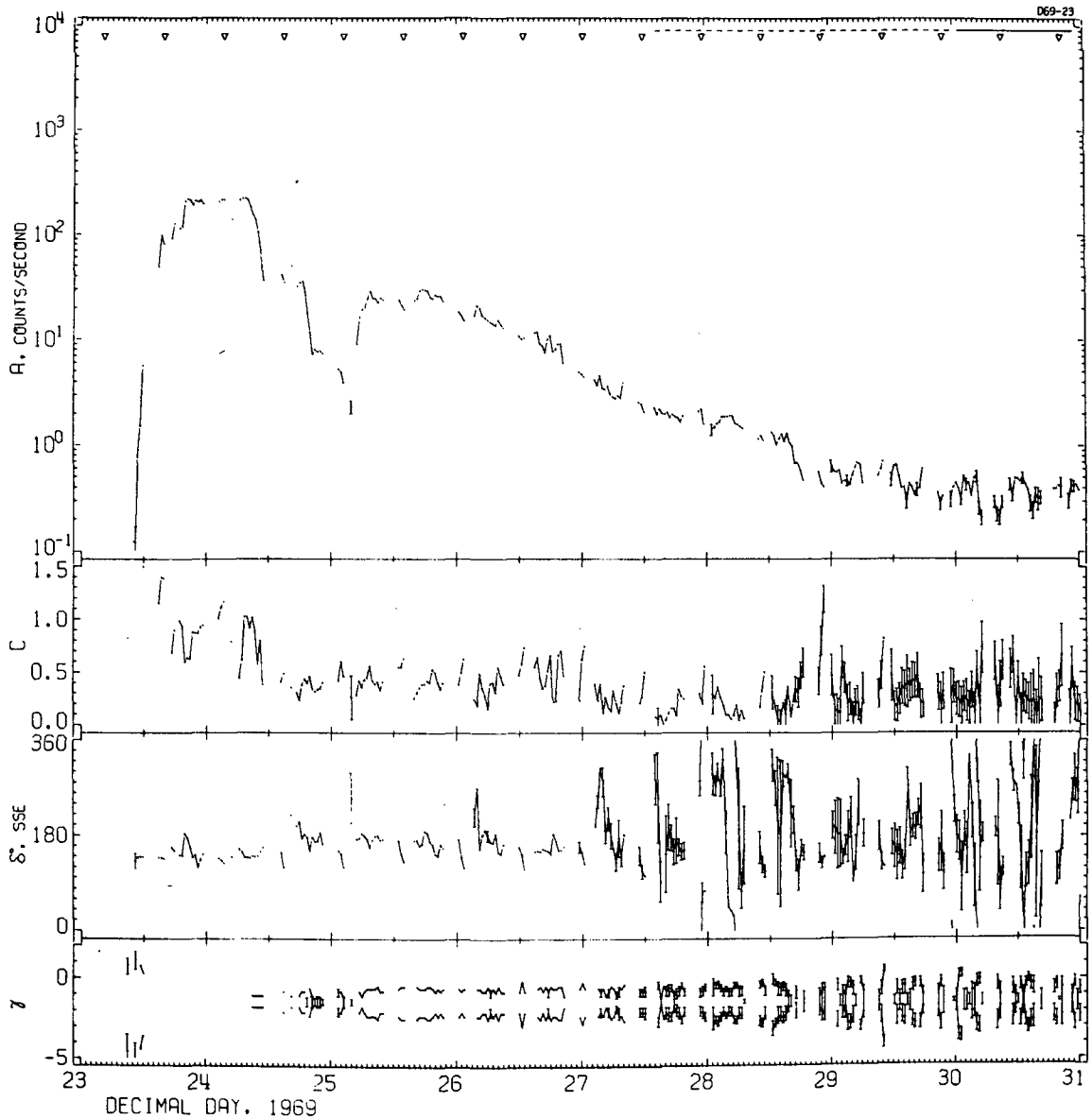

Figure 10

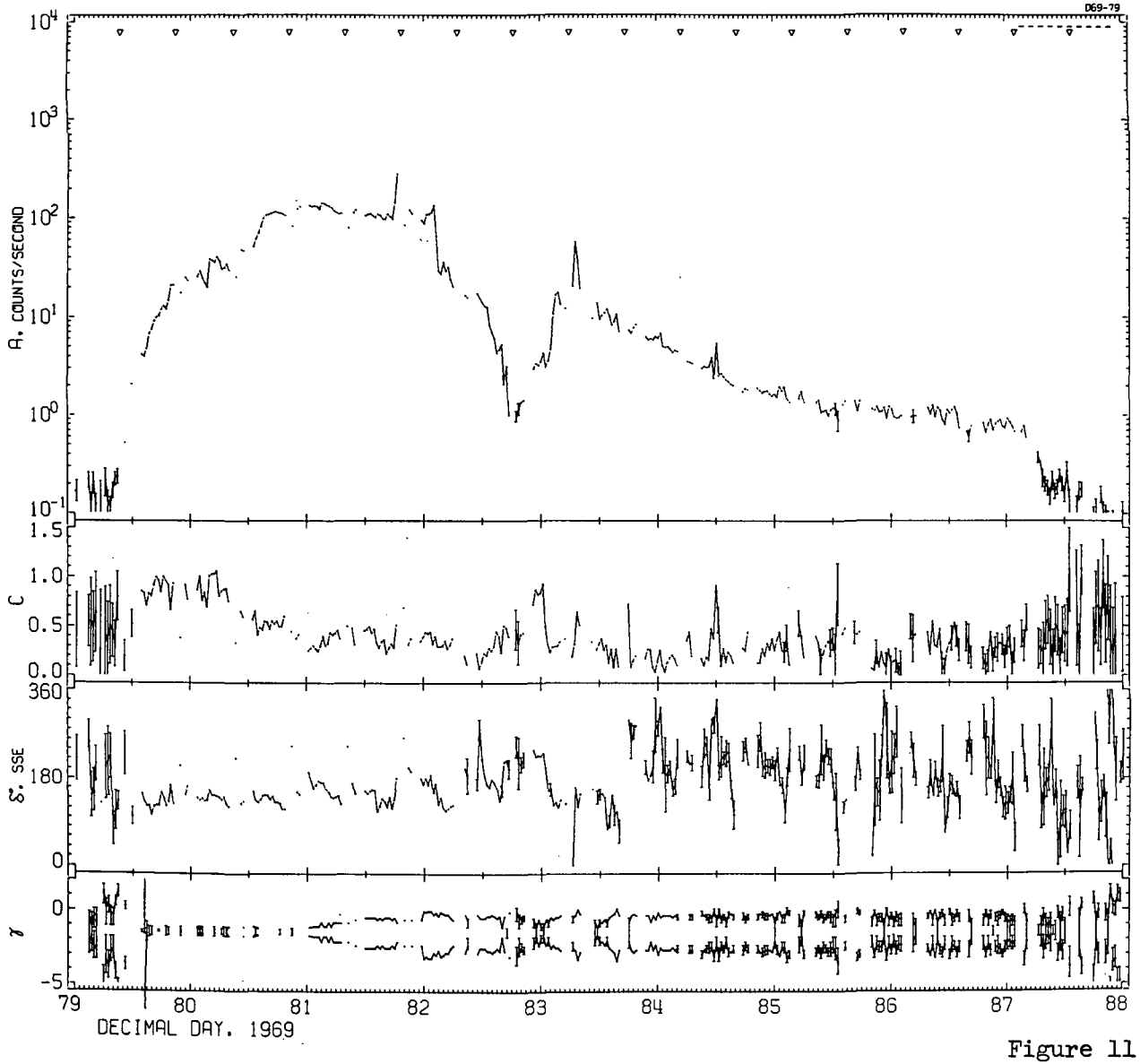

Figure 11

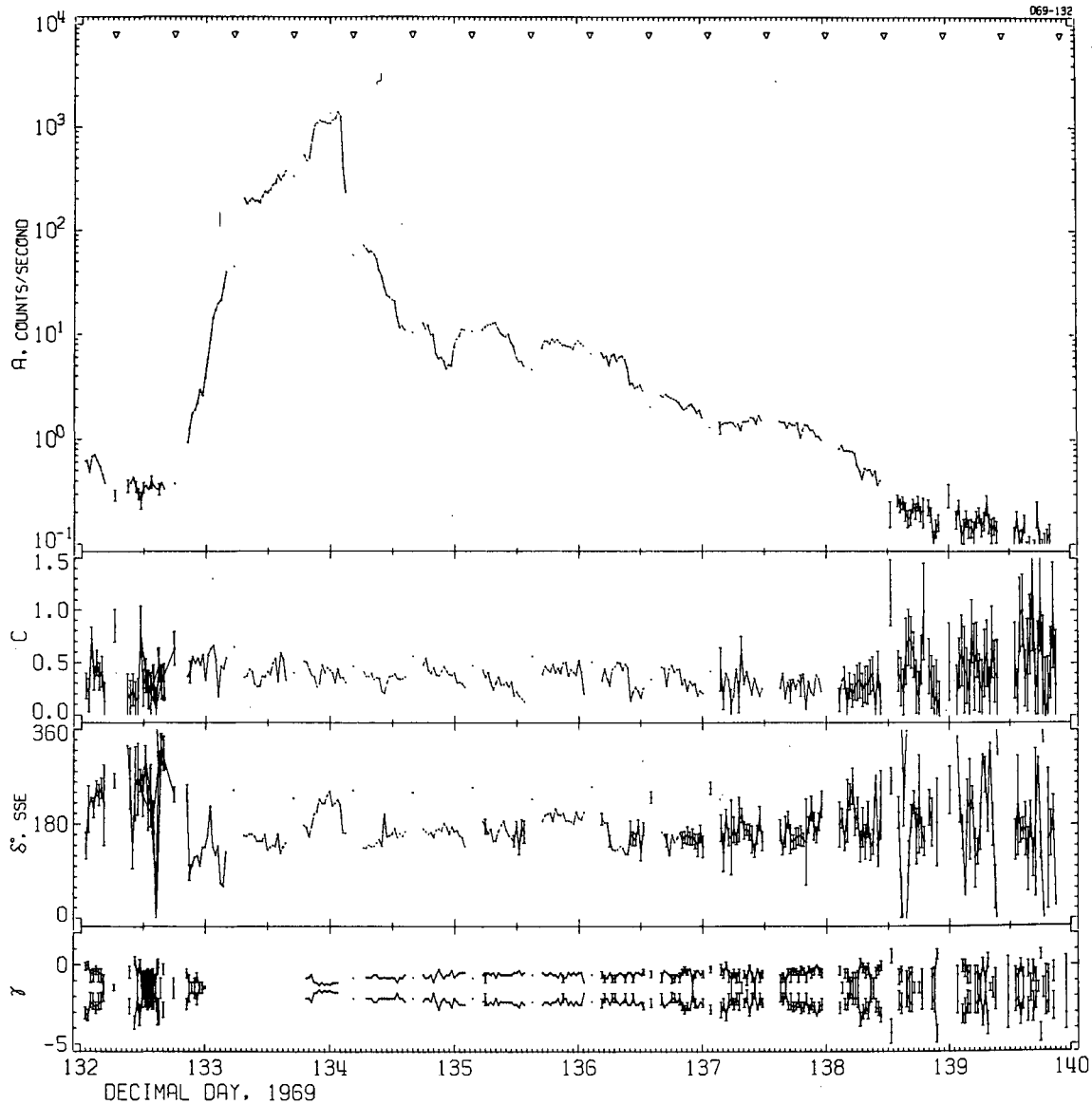

Figure 12

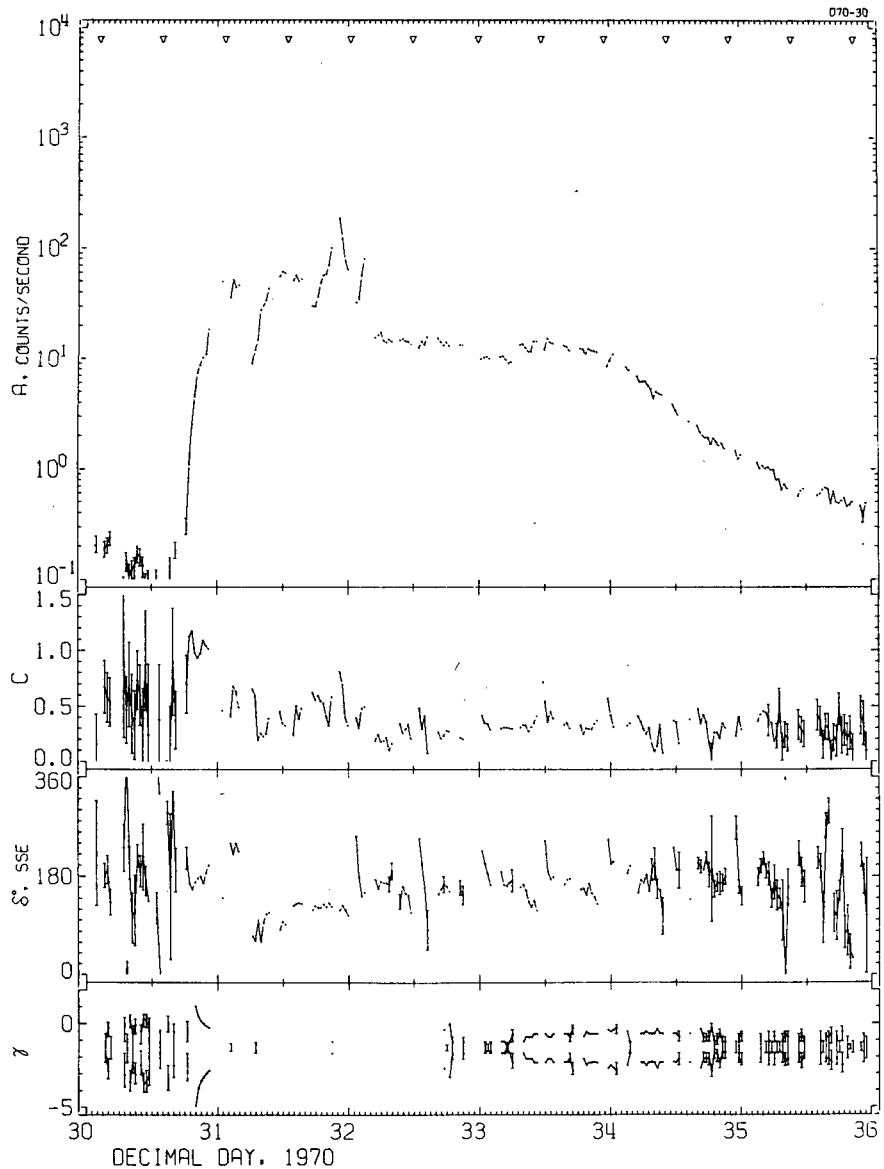

Figure 13

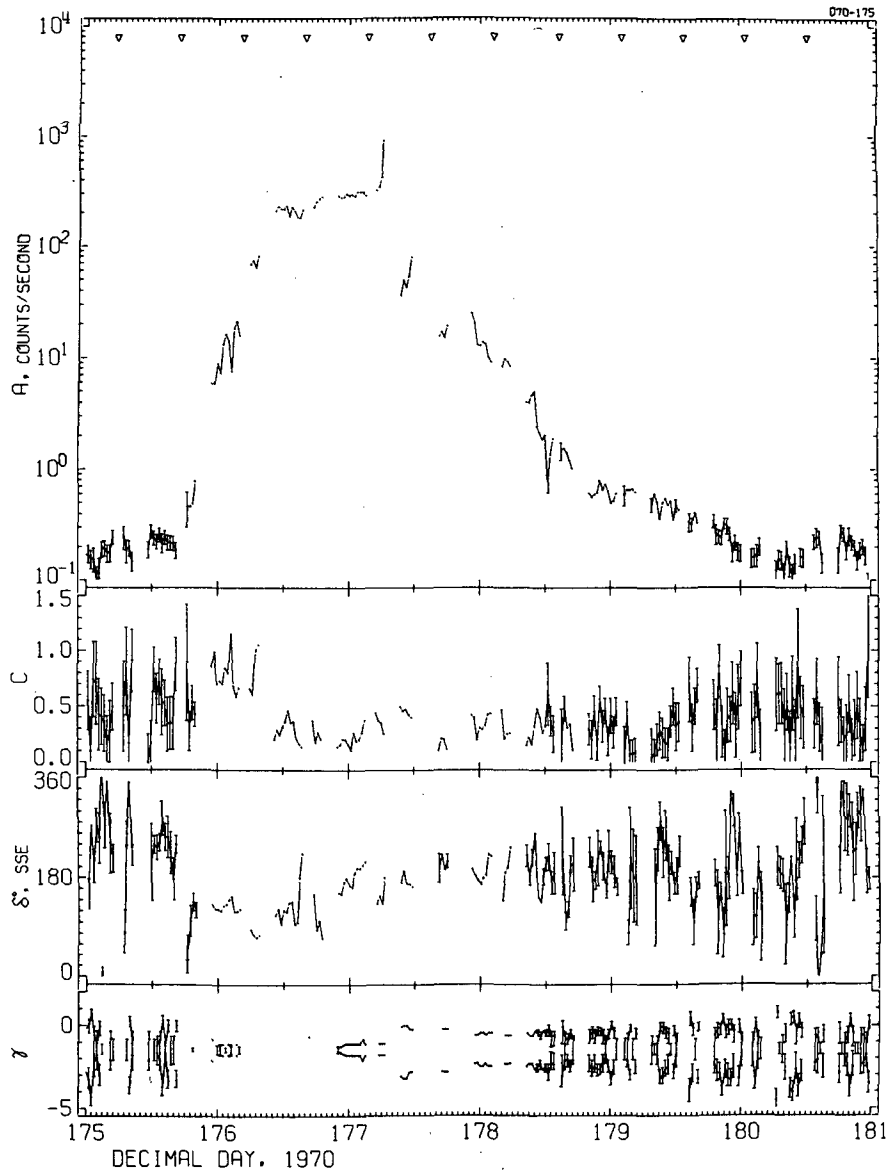

Figure 14

A-G72-273

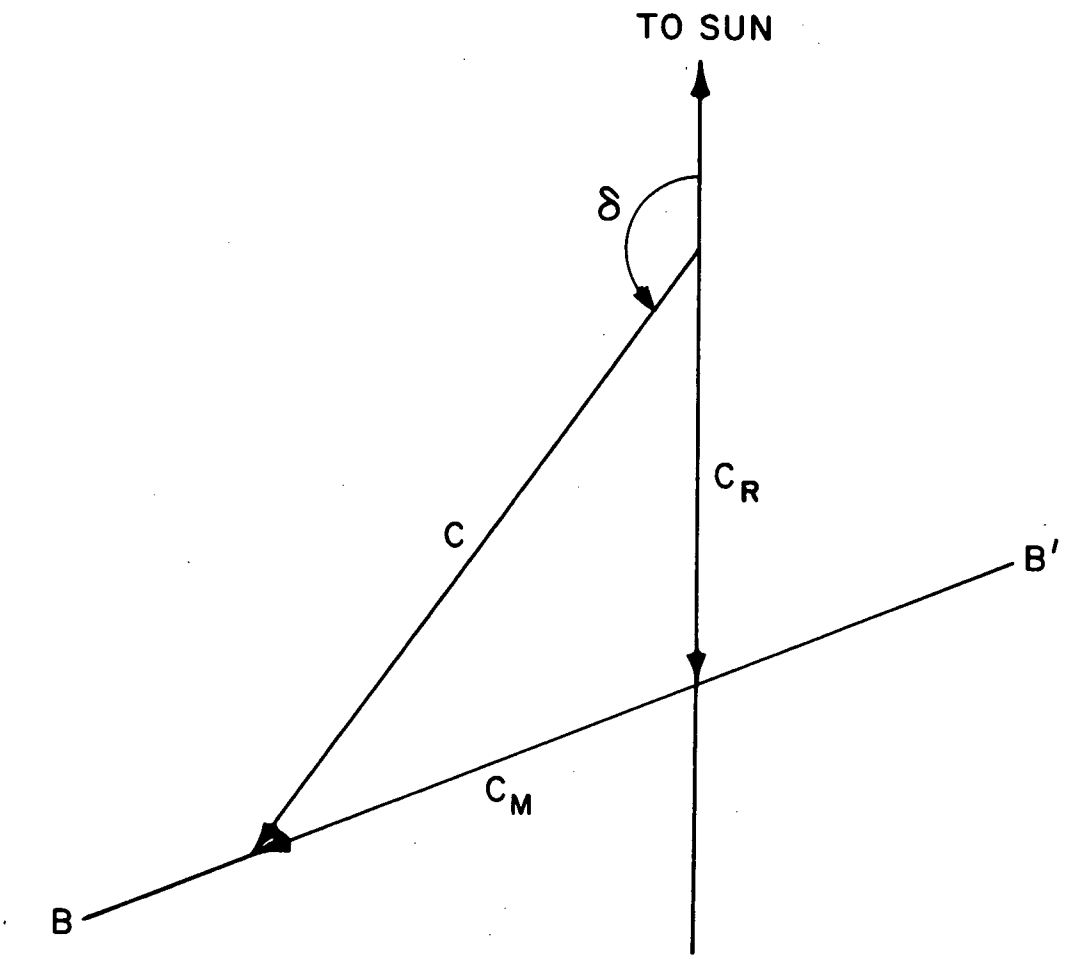

Figure 15

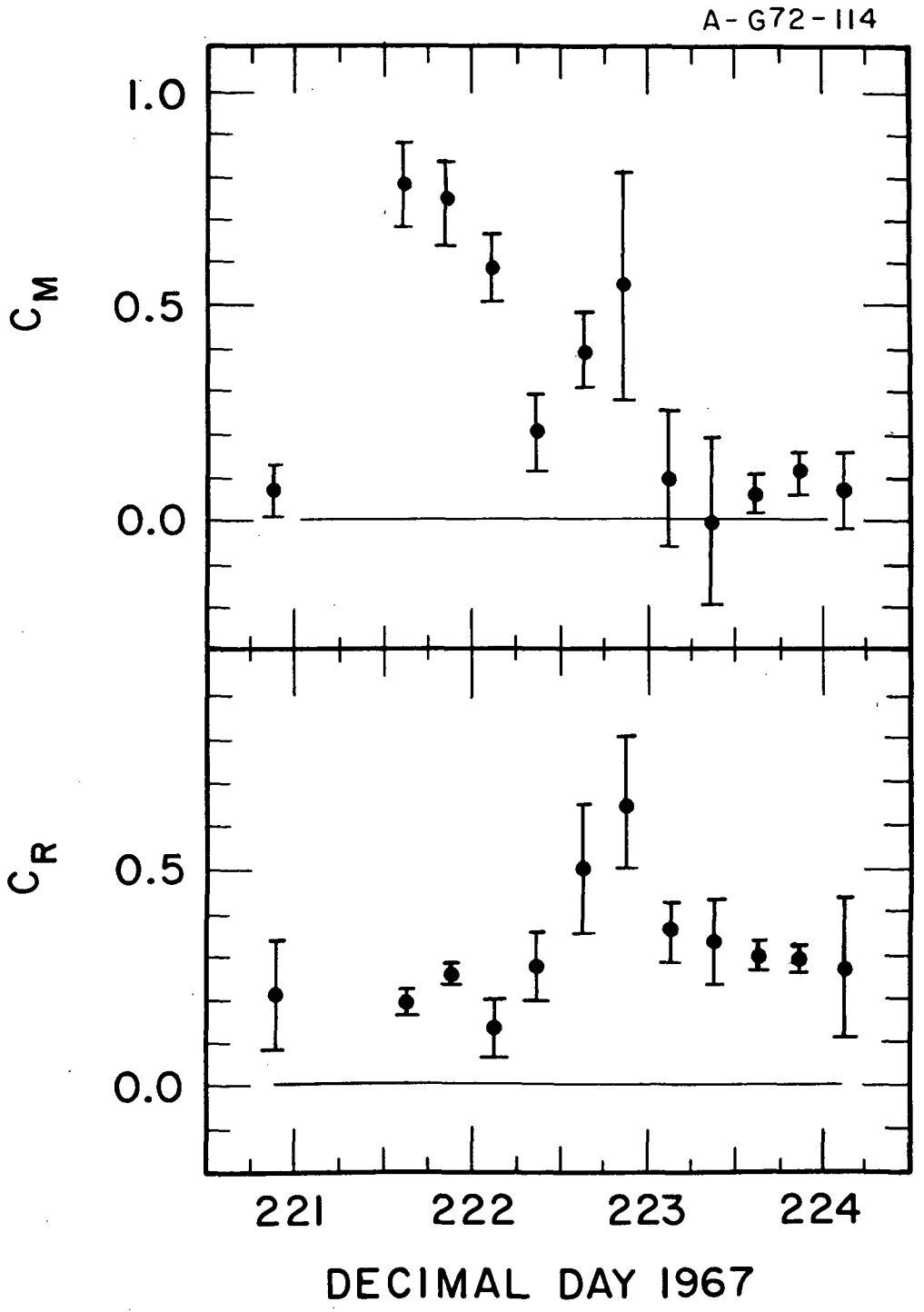

Figure 16

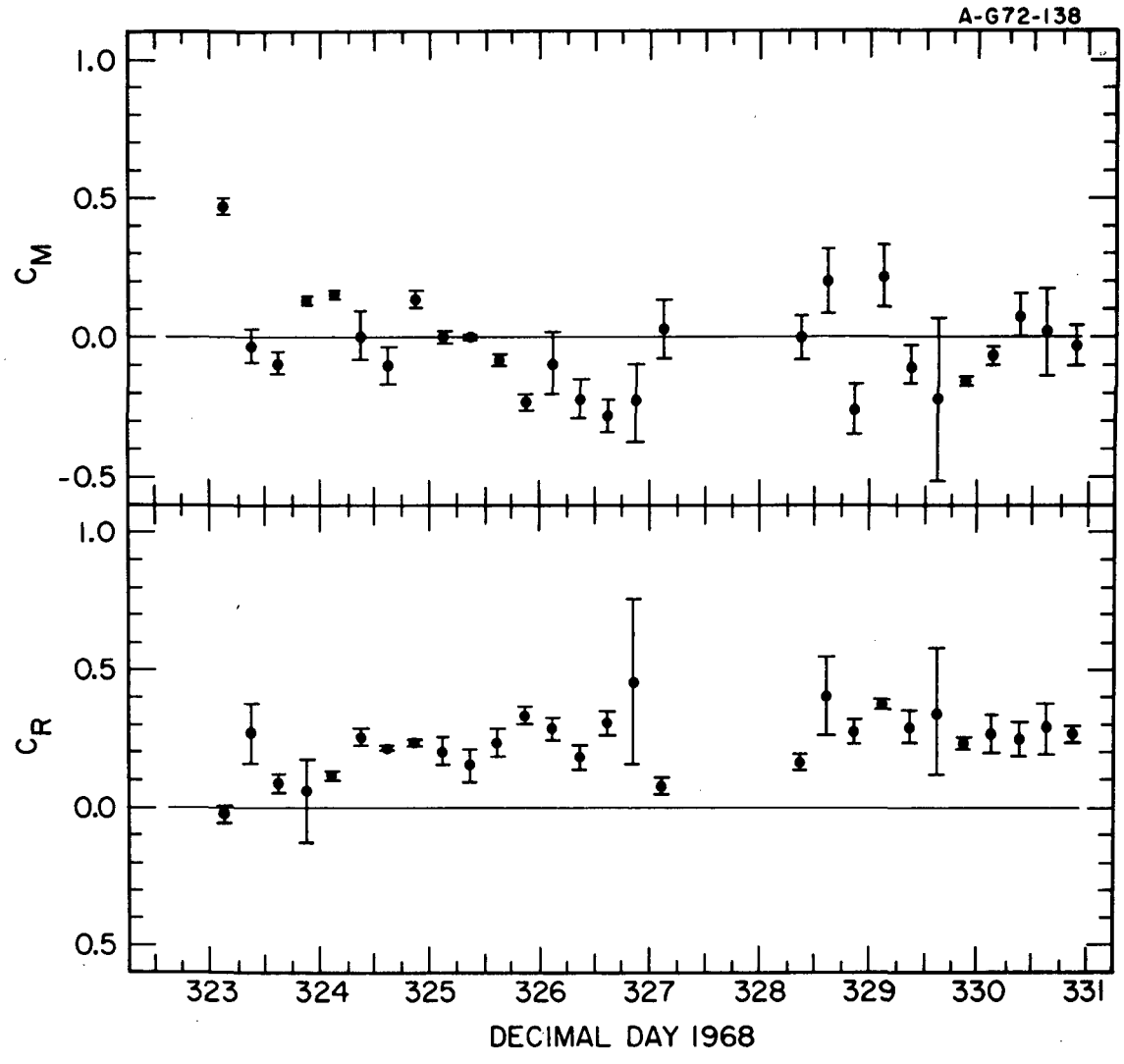
A-G72-138
1.0
0.5
0.0
-0.5
C_M
1.0
0.5
0.0
0.5
C_R
323
324
325
326
327
328
329
330
331
DECIMAL DAY 1968

Figure 17

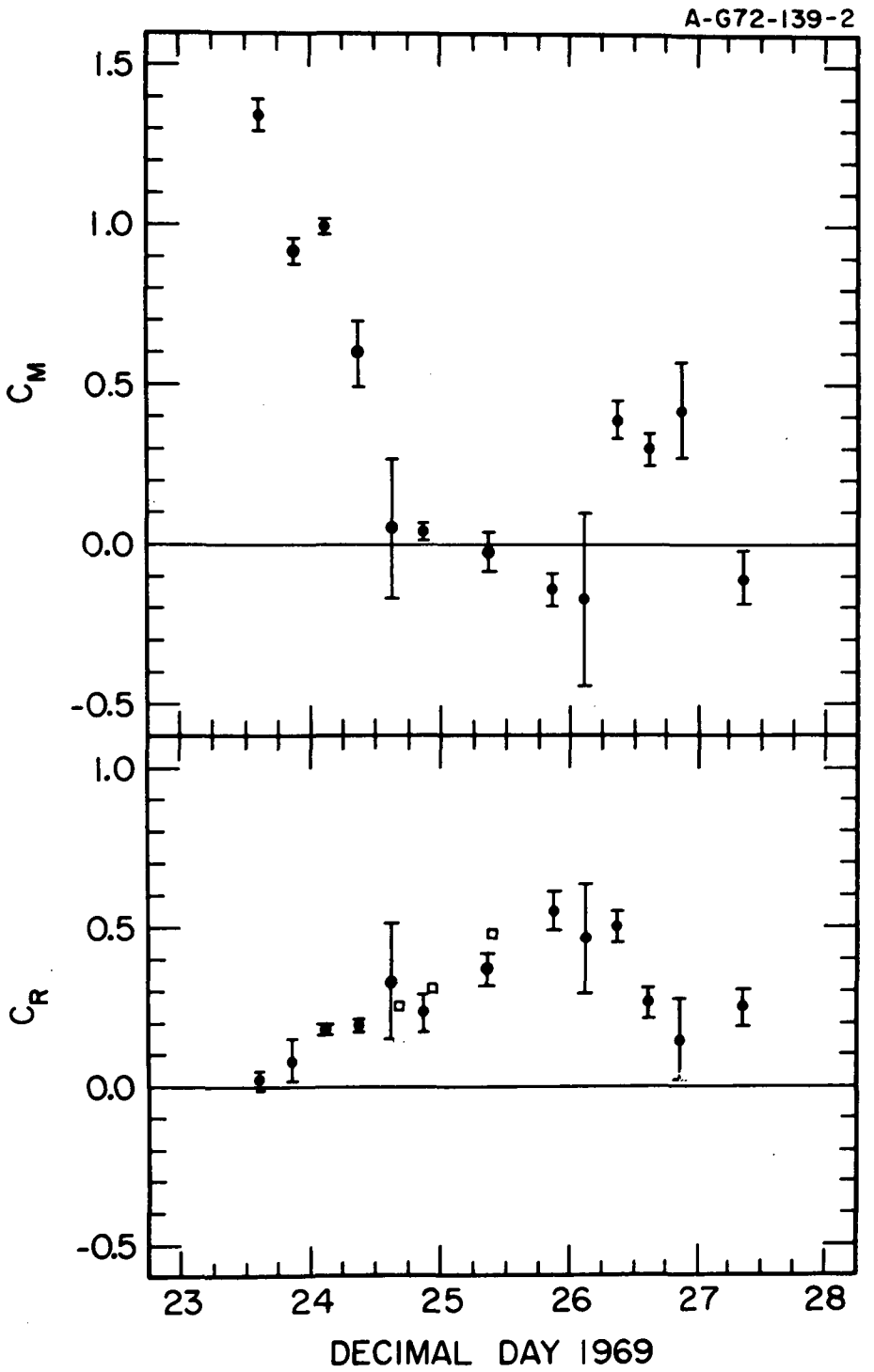
A-G72-139-2
1.5
1.0
0.5
0.0
-0.5
C_M
1.0
0.5
0.0
-0.5
C_R
23
24
25
26
27
28
DECIMAL DAY 1969

Figure 18

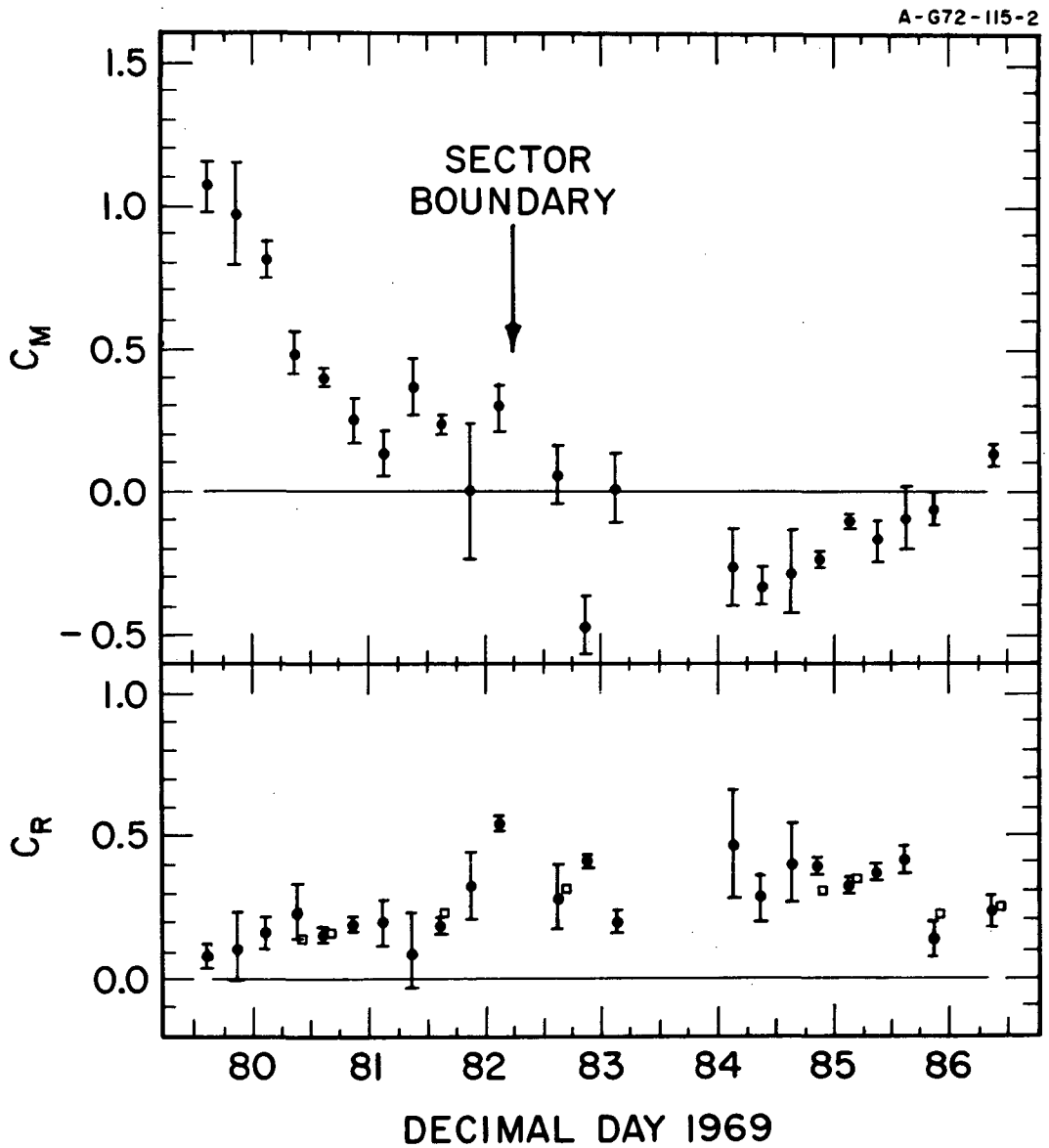
A-G72-115-2
1.5
1.0
0.5
0.0
-0.5
SECTOR
BOUNDARY
C_M
1.0
0.5
0.0
C_R
80
81
82
83
84
85
86
DECIMAL DAY 1969

Figure 19

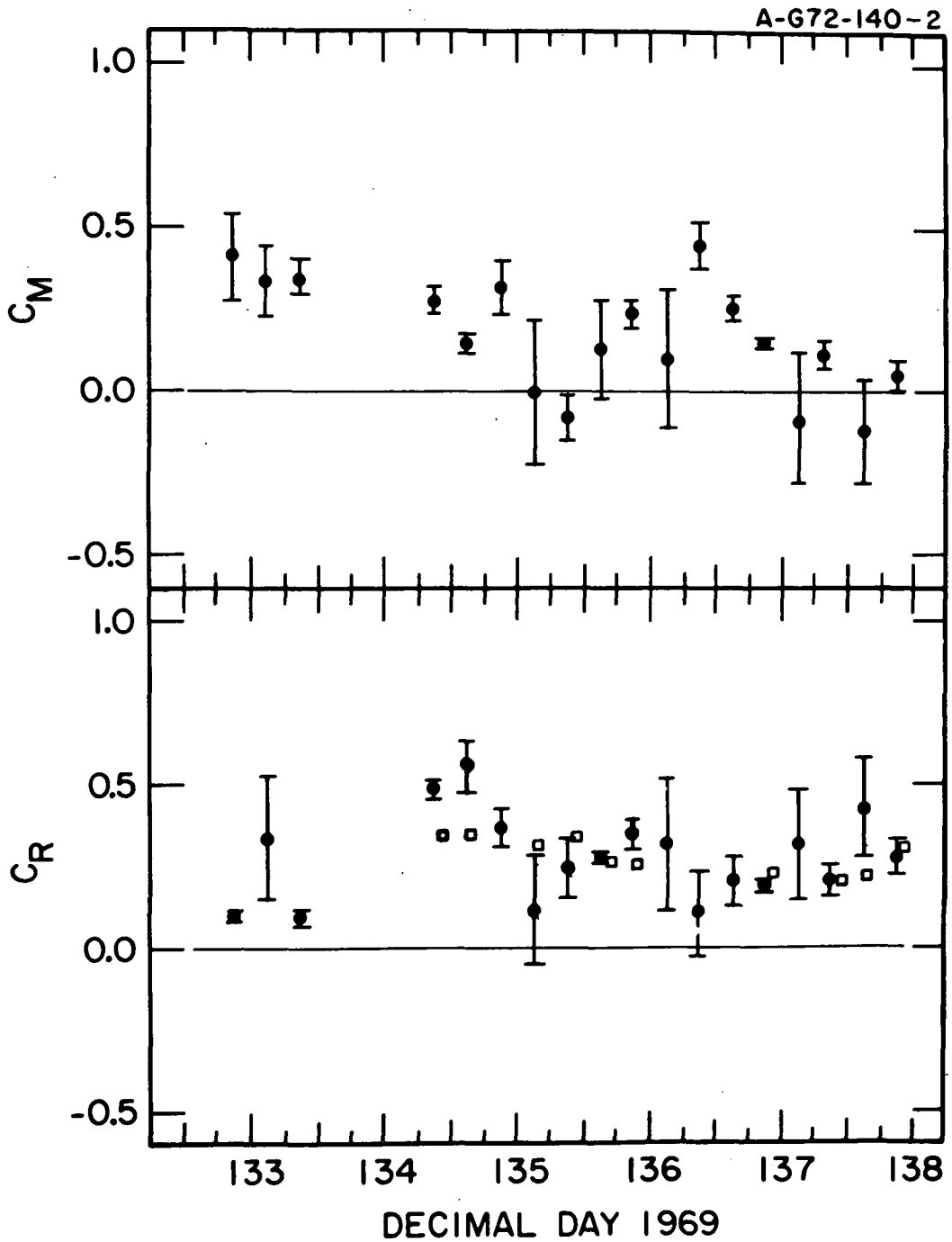
A-G72-140-2
1.0
0.5
0.0
-0.5
C_M
1.0
0.5
0.0
-0.5
C_R
133
134
135
136
137
138
DECIMAL DAY 1969

Figure 20

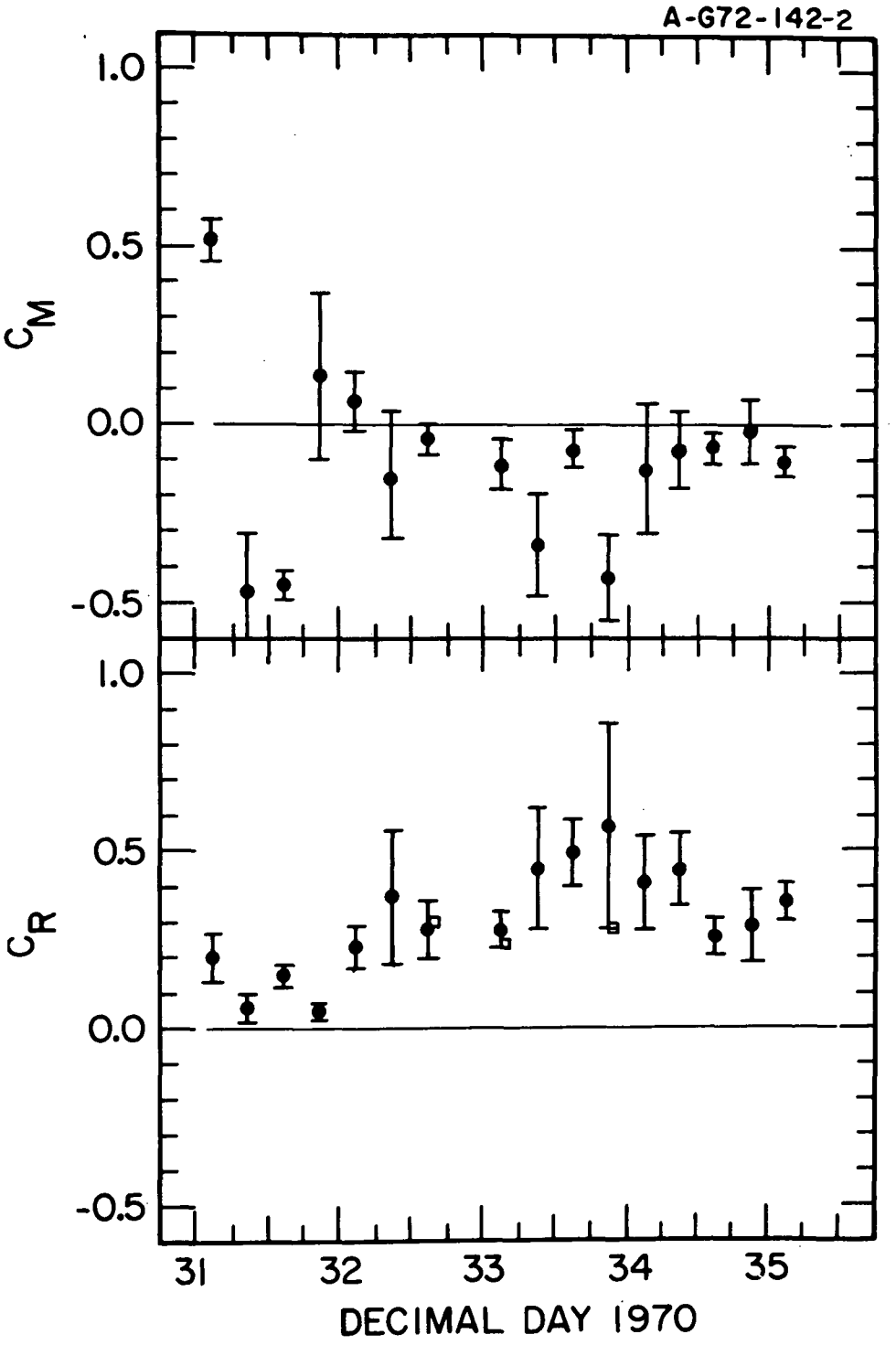
A-G72-142-2
1.0
0.5
0.0
-0.5
C_M
1.0
0.5
0.0
-0.5
C_R
31
32
33
34
35
DECIMAL DAY 1970

Figure 21

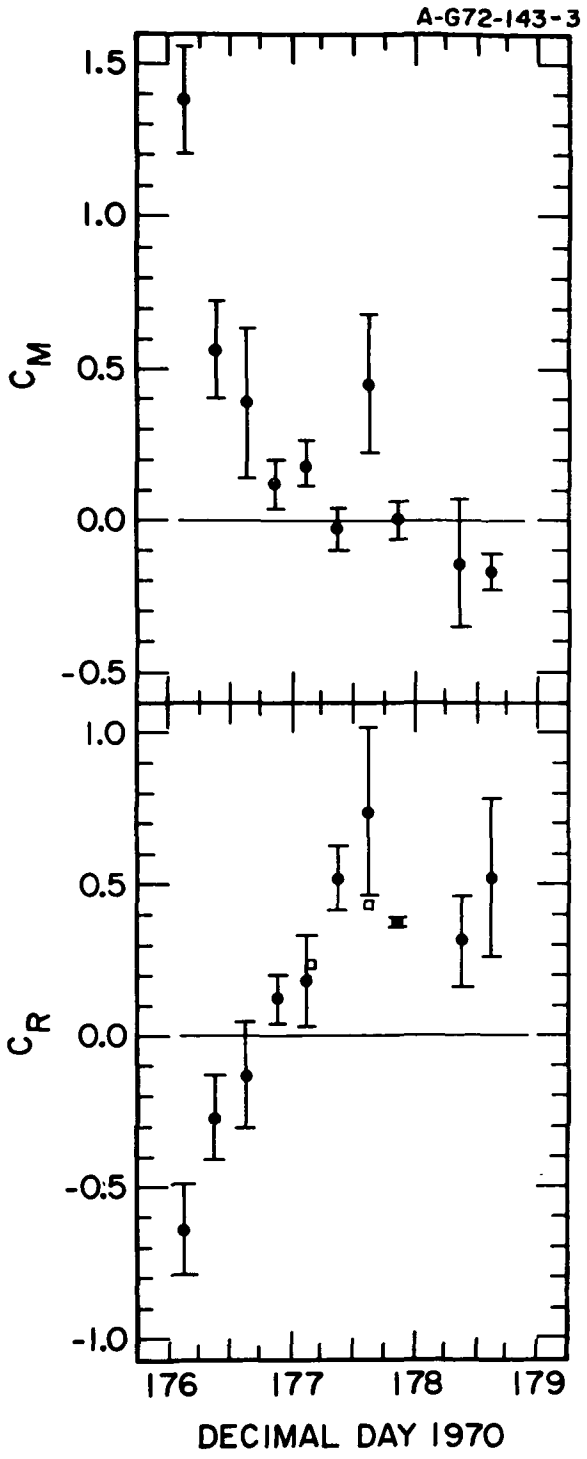
A-G72-143-3
1.5
1.0
0.5
0.0
-0.5
C_M
1.0
0.5
0.0
-0.5
-1.0
C_R
176
177
178
179
DECIMAL DAY 1970

Figure 22

DOCUMENT CONTROL DATA - R&D

(Security classification of title, body of abstract and indexing annotation must be entered when the overall report is classified)

1. ORIGINATING ACTIVITY (Corporate author)	2a. REPORT SECURITY CLASSIFICATION
Department of Physics and Astronomy University of Iowa	UNCLASSIFIED
	2b GROUP

3. REPORT TITLE

Anisotropies in the Interplanetary Intensity of Solar Protons $E_p > 0.3$ MeV

4. DESCRIPTIVE NOTES *(Type of report and inclusive dates)*

Progress, June 1972

5. AUTHOR(S) *(Last name, first name, initial)*

Innanen, William G., and Van Allen, James A.

6. REPORT DATE	7a. TOTAL NO. OF PAGES	7b. NO. OF REFS
June 1972	56	10

8a. CONTRACT OR GRANT NO.	9a. ORIGINATOR'S REPORT NUMBER(S)
N00014-68-A-0196-0003 b. PROJECT NO.	U. of Iowa 72-15
c. d.	9b. OTHER REPORT NO(S) *(Any other numbers that may be assigned this report)*

10. AVAILABILITY/LIMITATION NOTICES

Distribution of this document is unlimited.

11. SUPPLEMENTARY NOTES	12. SPONSORING MILITARY ACTIVITY
	Office of Naval Research

13. ABSTRACT

[See pages 2, 3, and 4 following]

DD FORM 1 JAN 64 1473

KEY WORDS	LINK A		LINK B		LINK C	
	ROLE	WT	ROLE	WT	ROLE	WT
Solar Protons						
Interplanetary Propagation						
Diffusive and Convective Transport						

INSTRUCTIONS

1. ORIGINATING ACTIVITY: Enter the name and address of the contractor, subcontractor, grantee, Department of Defense activity or other organization *(corporate author)* issuing the report.

2a. REPORT SECURITY CLASSIFICATION: Enter the overall security classification of the report. Indicate whether "Restricted Data" is included. Marking is to be in accordance with appropriate security regulations.

2b. GROUP: Automatic downgrading is specified in DoD Directive 5200.10 and Armed Forces Industrial Manual. Enter the group number. Also, when applicable, show that optional markings have been used for Group 3 and Group 4 as authorized.

3. REPORT TITLE: Enter the complete report title in all capital letters. Titles in all cases should be unclassified. If a meaningful title cannot be selected without classification, show title classification in all capitals in parenthesis immediately following the title.

4. DESCRIPTIVE NOTES: If appropriate, enter the type of report, e.g., interim, progress, summary, annual, or final. Give the inclusive dates when a specific reporting period is covered.

5. AUTHOR(S): Enter the name(s) of author(s) as shown on or in the report. Enter last name, first name, middle initial. If military, show rank and branch of service. The name of the principal author is an absolute minimum requirement.

6. REPORT DATE: Enter the date of the report as day, month, year; or month, year. If more than one date appears on the report, use date of publication.

7a. TOTAL NUMBER OF PAGES: The total page count should follow normal pagination procedures, i.e., enter the number of pages containing information.

7b. NUMBER OF REFERENCES: Enter the total number of references cited in the report.

8a. CONTRACT OR GRANT NUMBER: If appropriate, enter the applicable number of the contract or grant under which the report was written.

8b, 8c, & 8d. PROJECT NUMBER: Enter the appropriate military department identification, such as project number, subproject number, system numbers, task number, etc.

9a. ORIGINATOR'S REPORT NUMBER(S): Enter the official report number by which the document will be identified and controlled by the originating activity. This number must be unique to this report.

9b. OTHER REPORT NUMBER(S): If the report has been assigned any other report numbers *(either by the originator or by the sponsor)*, also enter this number(s).

10. AVAILABILITY/LIMITATION NOTICES: Enter any limitations on further dissemination of the report, other than those imposed by security classification, using standard statements such as:

(1) "Qualified requesters may obtain copies of this report from DDC."

(2) "Foreign announcement and dissemination of this report by DDC is not authorized."

(3) "U. S. Government agencies may obtain copies of this report directly from DDC. Other qualified DDC users shall request through _____."

(4) "U. S. military agencies may obtain copies of this report directly from DDC. Other qualified users shall request through _____."

(5) "All distribution of this report is controlled. Qualified DDC users shall request through _____."

If the report has been furnished to the Office of Technical Services, Department of Commerce, for sale to the public, indicate this fact and enter the price, if known.

11. SUPPLEMENTARY NOTES: Use for additional explanatory notes.

12. SPONSORING MILITARY ACTIVITY: Enter the name of the departmental project office or laboratory sponsoring *(paying for)* the research and development. Include address.

13. ABSTRACT: Enter an abstract giving a brief and factual summary of the document indicative of the report, even though it may also appear elsewhere in the body of the technical report. If additional space is required, a continuation sheet shall be attached.

It is highly desirable that the abstract of classified reports be unclassified. Each paragraph of the abstract shall end with an indication of the military security classification of the information in the paragraph, represented as *(TS), (S), (C), or (U)*.

There is no limitation on the length of the abstract. However, the suggested length is from 150 to 225 words.

14. KEY WORDS: Key words are technically meaningful terms or short phrases that characterize a report and may be used as index entries for cataloging the report. Key words must be selected so that no security classification is required. Identifiers, such as equipment model designation, trade name, military project code name, geographic location, may be used as key words but will be followed by an indication of technical context. The assignment of links, roles, and weights is optional.